



UNIVERSITÀ DI PARMA

ARCHIVIO DELLA RICERCA

University of Parma Research Repository

Dynamics of predator-prey models with a strong Allee effect on the prey and predator-dependent trophic functions

This is the peer reviewed version of the following article:

Original

Dynamics of predator-prey models with a strong Allee effect on the prey and predator-dependent trophic functions / Buffoni, Giuseppe; Groppi, Maria; Soresina, Cinzia. - In: NONLINEAR ANALYSIS: REAL WORLD APPLICATIONS. - ISSN 1468-1218. - 30:(2016), pp. 143-169. [10.1016/j.nonrwa.2015.12.001]

Availability:

This version is available at: 11381/2808162 since: 2021-10-07T12:23:58Z

Publisher:

Elsevier Ltd

Published

DOI:10.1016/j.nonrwa.2015.12.001

Terms of use:

Anyone can freely access the full text of works made available as "Open Access". Works made available


Publisher copyright

note finali coverpage

(Article begins on next page)

18 April 2024

AUTHOR QUERY FORM

 ELSEVIER	Journal: Nonlinear Analysis: Real World Applications Article Number: 2389	Please e-mail your responses and any corrections to: E-mail: corrections.esch@elsevier.river-valley.com
--	--	--

Dear Author,

Please check your proof carefully and mark all corrections at the appropriate place in the proof (e.g., by using on-screen annotation in the PDF file) or compile them in a separate list. Note: if you opt to annotate the file with software other than Adobe Reader then please also highlight the appropriate place in the PDF file. To ensure fast publication of your paper please return your corrections within 48 hours.

For correction or revision of any artwork, please consult <http://www.elsevier.com/artworkinstructions>.

Location in article	Query / Remark click on the Q link to go Please insert your reply or correction at the corresponding line in the proof
<u>Q1</u>	Your article is registered as a regular item and is being processed for inclusion in a regular issue of the journal. If this is NOT correct and your article belongs to a Special Issue/Collection please contact p.mathias@elsevier.com immediately prior to returning your corrections.
<u>Q2</u>	Please confirm that given names and surnames have been identified correctly.
<u>Q3</u>	Please check the edit made here and correct if necessary.
<u>Q4</u>	An extra closing parenthesis has been inserted. Please check, and correct if necessary.
<u>Q5</u>	Please check the layout of Table 3, and correct if necessary.
<u>Q6</u>	Please provide grant number for 'MIUR', 'GNFM', 'University of Parma and Milano (Italy)' and 'CNR-IMATI'.
	<div style="border: 1px solid black; padding: 5px; display: inline-block;"> <p style="color: red; margin: 0;">Please check this box or indicate your approval if you have no corrections to make to the PDF file</p> <input style="width: 30px; height: 20px; vertical-align: middle;" type="checkbox"/> </div>

Thank you for your assistance.

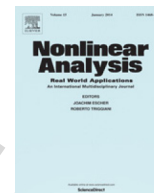


ELSEVIER

Contents lists available at ScienceDirect

Nonlinear Analysis: Real World Applications

www.elsevier.com/locate/nonrwa



Q1 Dynamics of predator–prey models with a strong Allee effect on the prey and predator-dependent trophic functions

Q2 G. Buffoni^a, M. Groppi^{b,*}, C. Soresina^c

^a CNR-IMATI, via Bassini 15, 20133 Milano, Italy

^b Dipartimento di Matematica e Informatica, Università di Parma, Parco Area delle Scienze 53/A, 43124 Parma, Italy

^c Dipartimento di Matematica “F. Enriques”, Università di Milano, via Cesare Saldini 50, 20133 Milano, Italy

ARTICLE INFO

Article history:

Received 9 December 2014

Received in revised form 27 October 2015

Accepted 12 December 2015

Available online xxxx

Keywords:

Predator–prey system

Allee effect

Predator-dependent trophic function

Stability

Bifurcations

ABSTRACT

The complex dynamics of a two-trophic chain are investigated. The chain is described by a general predator–prey system, in which the prey growth rate and the trophic interaction functions are defined only by some properties determining their shapes. To account for undercrowding phenomena, the prey growth function is assumed to model a strong Allee effect; to simulate the predator interference during the predation process, the trophic function is assumed predator-dependent. A stability analysis of the system is performed, using the predation efficiency and a measure of the predator interference as bifurcation parameters. The admissible scenarios are much richer than in the case of prey-dependent trophic functions, investigated in Buffoni et al. (2011). General conditions for the number of equilibria, for the existence and stability of extinction and coexistence equilibrium states are determined, and the bifurcations exhibited by the system are investigated. Numerical results illustrate the qualitative behaviours of the system, in particular the presence of limit cycles, of global bifurcations and of bistability situations.

© 2015 Published by Elsevier Ltd.

1. Introduction

This paper deals with the dynamics of a predator–prey system described in terms of a lumped parameter model [1,2], in which the demographic structure of the populations is neglected, in particular the stage structure for insects and mites (eggs, larvae, pupae, adults). Thus, the predator and prey populations may be characterized by just one state variable, representing their abundance in terms of biomass/spatial unit. Moreover, we assume a limited and controlled environment (for instance a greenhouse, in which temperature and humidity are maintained approximately constant) so that we can consider time independent bioecological parameters, and neglect the spatial distribution of the individuals.

* Corresponding author.

E-mail addresses: maria.groppi@unipr.it (M. Groppi), cinzia.soresina@unimi.it (C. Soresina).

In this framework, the local dynamics of a predator–prey system are mainly characterized by the formulations of the prey growth rate, in absence of predators, and of the prey consumption rate by predators. Let these rate be expressed as

$$\begin{aligned}\text{prey growth rate} &= XG(X), \\ \text{prey consumption rate} &= YF(X, Y),\end{aligned}$$

where X and Y are prey and predator abundances. The model functions $G(X)$ and $F(X, Y)$ are specific rates and their shapes determine the type of prey growth and predation processes, respectively. They strongly depend on the basic assumptions made on the bioecological processes to be simulated and their shape is often unknown, thus only some of their qualitative properties can be specified. The main purpose of this work is to investigate the dynamical behaviours of a predator–prey system, when the model functions describing the biological processes occurring in the considered trophic chain are not specified by analytical expressions, but by some characteristic properties determining their shapes. It will be shown that this is feasible for the existence and stability analysis of the equilibrium states of the system: indeed, existence and stability conditions of the equilibrium states can be established in a general framework in terms of some crucial parameters. Unfortunately, the stability analysis of limit cycles cannot be easily performed following this general approach, and the model functions have to be specified to go further in the qualitative analysis.

The general properties of $G(X)$ and $F(X, Y)$ assumed in this work are here enlightened. We will consider non-monotonic $G(X)$ accounting for undercrowding and extinction phenomena, suitable to model a strong Allee effect (see for instance [3–8]). $G(X)$ should be negative and increasing for sufficiently small X ; positive between K^- , referred to as the minimum population size ([9]; [10], p. 275), and K^+ , often referred to as the carrying capacity of the environment [11, p. 26]; negative and non-increasing for sufficiently large X . A brief review of the formulations of the prey growth rate in the development of predator–prey theory, together with analytical expressions of $G(X)$ proposed in the literature and used in the applications to simulate both strong and weak Allee effects, can be found for instance in [12].

$F(X, Y)$ is called the trophic function and describes the predator functional response to prey abundance [11, p. 80]. It was introduced in predator–prey models to take into account the saturation limiting the predation process. To have a biologically meaningful interpretation some qualitative assumptions on $F(X, Y)$ about the dependence on X and Y have to be required:

$$\begin{aligned}F(X, Y) > 0 \quad X > 0, Y \geq 0, \quad F(0, Y) = 0, \quad \lim_{X \rightarrow +\infty} F(X, Y) < +\infty \\ \frac{\partial F}{\partial X} > 0, \quad \frac{\partial F}{\partial Y} < 0.\end{aligned}$$

At first, the trophic function was assumed to be dependent only on prey abundance ([13–16] and [11, p. 109–112]). Moreover, the Holling-type II [14] or the Ivlev type [15,16] models were introduced to simulate the saturation effect of the predation process. This formulation of F only in terms of X gives rise to the “paradoxes of enrichment and biological control” [17–19], and it is unable to generate the outcome of the extinction of the two populations [17] without taking into account a strong Allee effect in the prey growth [20].

Later, the notion of per-capita availability of food was introduced. It was suggested that the trophic function should be expressed in terms of the ratio X/Y of prey to predator abundance [17,19,21]:

$$F(X, Y) = bf(PX/Y), \quad (1)$$

where b is the maximum prey consumption rate and P is referred to as the efficiency of the predation process. This formulation solves the above-mentioned paradoxes, and in addition allows to describe experimental observations, in particular the extinction of predator or both prey and predator populations, without

resorting to the Allee effect. However, in this approach the trophic function has a singularity in the origin $X = 0, Y = 0$. This problem is solved by some authors by the blow-up method [22] or by a time rescaling [23]. Some other authors [24] modified the ratio X/Y by adding a small constant A in the denominator, so that they wrote $f(PX/(Y + A))$, and this trick [24] “...would alleviate the problem. Although this addition may appear difficult to justify biologically, Gutierrez [21] used an exponent of this form in his functional response term” of Ivlev type. It is worth noticing that the total extinction is a possible outcome when $A = 0$, while it cannot be obtained with this non-singular trophic function for any $A > 0$, as treated in detail in [25]. The efficiency P in (1) is assumed to be constant by some authors in their models [17,22,19]. On the other hand, it could be assumed predator-dependent [26–29]: $P(Y)$ has to increase with Y , with a saturation effect for increasing Y due to the predator interference during foraging, and $P(Y)/Y$ has to decrease with Y to satisfy $\partial F/\partial Y < 0$. Note that, under the assumption that $P(Y) \propto Y$ as $Y \rightarrow 0$, the trophic function is no more singular in the origin. Different formulations have been proposed in the literature for $f(P(Y)X/Y)$. Gutierrez et al. [29] proposed an Ivlev-type formulation for both $f(\cdot)$ and $P(\cdot)$, while Beddington, DeAngelis and coauthors [26–28,30] proposed a Holling-type II for both $f(\cdot)$ and $P(\cdot)$.

In this paper we will study a predator–prey model which includes a strong Allee effect in the prey growth and a predator-dependent trophic function given by

$$F(X, Y) = bf \left(\frac{P_0 X}{K_0 + H_0 Y} \right), \quad (2)$$

where K_0 is a reference biomass, P_0 and H_0 are adimensional parameters: P_0 denotes the predation efficiency and H_0 is a measure of the predator interference process. Regarding the trophic function $f(\cdot)$, we prefer, until it is feasible, to introduce just one argument, instead of using a two-arguments function; this allows us to formulate its properties in a more concise form.

The paper is organized as follows. In Section 2 the basic assumptions and equations for the local dynamics of a predator–prey system are presented: the equations are written in terms of the adimensional variables X/K^+ and Y/K^+ , the growth of the prey takes into account a strong Allee effect, and the interactions between prey and predator are determined by a trophic function as in (2). In Section 3 the stability properties of the non-coexistence equilibrium states are summarized. In Sections 4 and 5 an existence and stability analysis of the coexistence equilibrium states is performed: parameters related to P_0 and H_0 will be assumed as bifurcation ones. In Section 6 results of numerical simulations, obtained for some concrete realization of the model functions, are presented to illustrate the behaviours of the system. Such results confirm analytical predictions and throw light on some aspects of the dynamics of the system. In Section 7 some concluding remarks can be found and results are commented on with reference to the existing literature. For the readers’ convenience, the symbols used in this paper have been collected in Appendix A; in Appendix B details on some crucial parameters can be found and in Appendix C technical details of the stability analysis of coexistence equilibrium states are reported.

2. Basic assumptions and model equations

Let

$$x = \frac{X}{K^+}, \quad y = \frac{Y}{K^+}, \quad p = P_0 \frac{K^+}{K_0}, \quad h = H_0 \frac{K^+}{K_0}.$$

Then, setting the prey growth rate $G = r_x g(x)$, where r_x is the maximum specific growth rate of the prey, and taking into account the expression (2) for the trophic function, the balance equations for the local

dynamics of the two trophic levels in a controlled environment are written as

$$\begin{cases} \frac{dx}{dt} = r_x x g(x) - b y f\left(\frac{px}{1+hy}\right) \\ \frac{dy}{dt} = c b y f\left(\frac{px}{1+hy}\right) - m y \\ x(0) = \tilde{x}, \quad y(0) = \tilde{y}, \end{cases} \quad (3)$$

where b , m are specific rates, c is a conversion factor, and p and h are adimensional parameters referred to as predation efficiency and predator interference during the predation process. The functions $g(\cdot)$ and $f(\cdot)$ should satisfy some regularity and general assumptions dictated by biological considerations. It is assumed that

$$\exists \epsilon : 0 < \epsilon < 1, \quad g(\epsilon) = g(1) = 0; \quad g(s)(s - \epsilon)(1 - s) > 0, \quad s \neq \epsilon, 1; \quad (4)$$

$$f(0) = 0, \quad \lim_{s \rightarrow +\infty} f(s) = 1, \quad f'(s) > 0, \quad s > 0. \quad (5)$$

The parameter ϵ is the ratio between minimum and maximum population size

$$\epsilon = K^- / K^+.$$

Hereafter the prime indicates the derivative with respect to the argument. Moreover, some further technical assumptions on the smoothness of these functions are required to limit the number of equilibrium states of (3) and to make the stability analysis tractable. We will assume: (i) just one maximum when $g(s)$ is positive, (ii) just one inflection point of $sg(s)$ when $g(s)$ is positive and increasing, (iii) a weaker than negative convexity when $g(s)$ is positive and decreasing and (iv) a weaker than negative convexity for $f(s)$. These conditions can be written as

$$\exists \xi_0 : \epsilon < \xi_0 < 1, \quad g(\xi_0) = 1, \quad g'(\xi_0) = 0; \quad g'(s)(\xi_0 - s) > 0, \quad \epsilon < s < 1, \quad s \neq \xi_0; \quad (6)$$

$$\exists \eta_0 : \epsilon < \eta_0 < \xi_0, \quad [sg(s)]''_{s=\eta_0} = 0; \quad [sg(s)]''(\eta_0 - s) > 0, \quad \epsilon < s < \xi_0, \quad s \neq \eta_0; \quad (7)$$

$$[sg'(s)]' < 0, \quad \xi_0 < s \leq 1; \quad (8)$$

$$\left[\frac{f(s)}{s}\right]' < 0, \quad s > 0. \quad (9)$$

The required properties (4)–(9) are fulfilled for instance by the following model functions, widely used in literature (see references in [12]):

$$\text{Prey growth:} \quad g(s) = g_0(s - \epsilon)(1 - s), \quad (10)$$

$$g(s) = g_0 \left(s \exp\left(\frac{1-s}{s}\right) - 1 \right), \quad (11)$$

$$\text{Trophic Functions:} \quad f(s) = \frac{s}{1+s}, \quad (12)$$

$$f(s) = 1 - \exp(-s), \quad (13)$$

where g_0 is such that $g(\xi_0) = 1$. The function (10) is the Gilpin model [5], (11) is from [12], (12) is the Holling-type II trophic function [14] and (13) is the Ivlev model [15,16].

Remarks. (I) The function $g(s)$ is normalized so that $g(\xi_0) = 1$, in order to have r_x as the maximum specific growth rate.

(II) The expression in conditions (7) and (8) can be written as

$$[sg(s)]'' = \frac{1}{s} [s^2 g'(s)]' = 2g'(s) + sg''(s), \quad [sg'(s)]' = g'(s) + sg''(s).$$

Thus, for $\xi_0 < s \leq 1$, namely when $g(s)$ is positive and decreasing, condition (8) is stronger than (7).

(III) Conditions (8) and (9) are weaker than $g''(s) < 0$ and $f''(s) < 0$, respectively. In fact, when $g'(s) < 0$, as it is in the interval $(\xi_0, 1]$, we have that $g''(s) < 0 \Rightarrow [sg'(s)]' < 0$. Moreover, when $f'(s) > 0$, we have that $f''(s) < 0 \Rightarrow [f(s)/s]' < 0$. The concavity of $f(s)$ may be positive with some restrictions: the inflection points, when they exist, should have tangent lines intersecting the vertical axes.

We are interested in positive solutions to (3). It is possible to show that all solutions initiating in \mathbb{R}_2^+ are bounded and eventually enter an attracting set.

Theorem 1. Under the assumptions (4) and (5) the closed set

$$\Omega = \left\{ (x, y) \in \mathbb{R}_2^+ \mid 0 \leq x \leq 1, 0 \leq x + \frac{y}{c} \leq 1 + \frac{r_x}{m} \right\}$$

is positively invariant, and for all initial states $\tilde{E} = (\tilde{x}, \tilde{y}) \in \mathbb{R}_2^+$ the trajectory $(x(t), y(t))$ eventually enters into Ω as $t \rightarrow +\infty$.

The proof is a straightforward application of the comparison theorem for ODE's and makes use of suitable bounds for the right hand side of (3) [31].

3. Non-coexistence equilibrium states and their stability properties

The existence and stability analysis of the non-negative equilibrium states $E = (x_{eq}, y_{eq})$ for the system (3) is performed assuming the parameters h and p as bifurcation parameters, while the remaining parameters are fixed.

For any $h \geq 0$ and $p > 0$, the system admits as equilibrium states the null state $E_0 = (0, 0)$ and, under the assumptions (4) on $g(\cdot)$, two non-coexistence states:

$$E_\epsilon = (\epsilon, 0), \quad E_1 = (1, 0).$$

Let r_y be the maximum specific growth rate of the predator. From (3) and (5) we have that

$$r_y = cb - m = cb(1 - \alpha), \quad \text{with } \alpha = \frac{m}{cb}. \quad (14)$$

If $r_y < 0$, i.e. $\alpha > 1$, then $y'(t) < 0$ for any $x, y > 0$. Thus, coexistence equilibrium states cannot exist. $y(t)$ is always decreasing and, as $t \rightarrow +\infty$, it can be easily seen that $(x(t), y(t))$ converges to either E_0 or E_1 , depending on the initial conditions. In the following, we will assume $r_y > 0$, i.e.

$$\alpha < 1. \quad (15)$$

In this case, the following implication holds

$$r_y > 0 \implies \exists p_0 = f^{-1}(\alpha) > 0, \quad (16)$$

and p_0 turns out to be a critical value of p for the existence and stability of the equilibrium states associated with (3). It depends only on the ratio α : $p_0 = p_0(\alpha)$, and we have

$$\frac{dp_0}{d\alpha} > 0, \quad p_0(0) = 0, \quad \lim_{\alpha \rightarrow 1} p_0(\alpha) = +\infty.$$

According to the Hartman–Grobman Theorem [32], the local stability properties of the equilibrium states E_ν , $\nu = 0, \epsilon, 1$, are determined by the analysis of the eigenvalues of the Jacobian matrix associated with system (3)

$$J(x, y) = \begin{pmatrix} r_x g(x) + r_x x g'(x) - bp u f'(pv) & -bf(pv) + bph u v f'(pv) \\ cbp u f'(pv) & cbf(pv) - m - cbph u v f'(pv) \end{pmatrix}$$

where

$$u = \frac{y}{1 + hy}, \quad v = \frac{x}{1 + hy},$$

and evaluated in E_i . Such eigenvalues, and then the stability properties of the non-coexistence states, turn out to be independent of h . Moreover, it follows that the stability properties of E_0 and E_ϵ are independent of p , while those of E_1 depend on p . The classification of the non-coexistence equilibrium states is the following:

E_0 is a locally stable node for any $p > 0$;

E_ϵ is always unstable: it is a saddle for $p < p_0/\epsilon$ (with unstable manifold $W_u(E_\epsilon)$ lying on the x -axis), and an unstable node for $p > p_0/\epsilon$;

E_1 is a locally stable node for $p < p_0$, and a saddle for $p > p_0$ (with stable manifold $W_s(E_1)$ lying on the x -axis).

4. Coexistence equilibrium states

Coexistence equilibrium states $E_*(h, p) = (x_*(h, p), y_*(h, p))$ are found as intersections of the nullclines of system (3), written as

$$y = \beta x g(x), \quad f\left(\frac{px}{1 + hy}\right) = \alpha, \quad (17)$$

where

$$\beta = \frac{r_x c}{m}.$$

It is worth noticing that the first nullcline in (17) is a humped curve in the phase plane, which is independent of parameters h and p . Under the assumption (15) and the definition (16) of p_0 , we have that the second nullcline in (17) is the straight line

$$\frac{p}{p_0} x = 1 + hy,$$

whose position and slope depend on both parameters h and p . Substituting y from the first equation in (17), we obtain the equation for x

$$\frac{p}{p_0} = \phi(x, h) = \frac{1}{x} + h\beta g(x). \quad (18)$$

We are interested in solutions to (18) $x_*(h, p) \in (\epsilon, 1)$, in order to have $y_*(h, p) > 0$. In fact, from the assumption (4), $g(x) > 0$ only in $(\epsilon, 1)$ and this implies that $p > p_0$. In the following we will assume $h > 0$. The case $h = 0$ has been studied in detail in [12].

4.1. Shape of $\phi(x, h)$

Q3 The shape of $\phi(x, h)$, and consequently the number of solutions to (18) in $(\epsilon, 1)$, strongly depend on the parameter h . We have

$$\frac{\partial \phi}{\partial x} = \frac{1}{x^2} [-1 + h\psi(x)], \quad \text{with } \psi(x) = \beta x^2 g'(x), \quad (19)$$

and

$$\frac{\partial \phi}{\partial h} = \beta g(x) > 0, \quad x \in (\epsilon, 1). \quad (20)$$

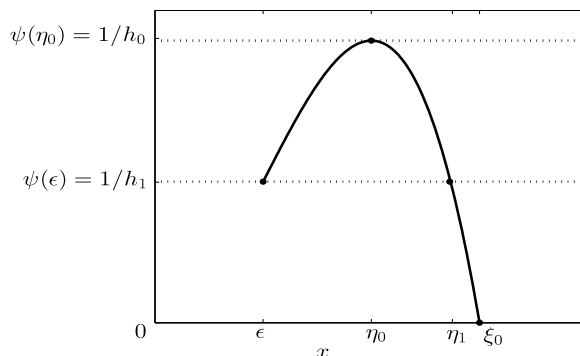
Fig. 1. Shape of the function $\psi(x)$.

Table 1

Number of solutions $\xi_j(h)$ to Eq. (21), and their positions on the x axis, for different ranges of h .

h	Number of solutions to $\partial\phi/\partial x = 0$	Position on the x axis
$0 \leq h < h_0$	0	
$h = h_0$	1	$\xi_2(h_0) = \eta_0 = \xi_1(h_0)$
$h_0 < h < h_1$	2	$\epsilon < \xi_2(h) < \eta_0 < \xi_1(h) < \eta_1$
$h = h_1$	2	$\epsilon = \xi_2(h_1) < \eta_0 < \xi_1(h_1) = \eta_1$
$h > h_1$	1	$\eta_1 < \xi_1(h) < \xi_0$

From the assumption (6), $g'(x) < 0$, and then $\partial\phi/\partial x < 0$, for $x \in (\xi_0, 1)$. Thus, $\phi(x, h)$ may be non-monotonic, with respect to x , only when $x \in (\epsilon, \xi_0)$ and $h \neq 0$. The points where $\partial\phi/\partial x = 0$ are solutions to the equation

$$\psi(x) = \frac{1}{h}, \quad h > 0. \quad (21)$$

We have $\psi(\epsilon) > 0$, $\psi(\xi_0) = 0$, and, from the assumption (7), $\psi(x)$ has only one maximum η_0 for $x \in (\epsilon, \xi_0)$. According to the shape of $\psi(x)$ (Fig. 1) in (ϵ, ξ_0) , it follows that there are two solutions to Eq. (21) when $\psi(\epsilon) \leq 1/h < \psi(\eta_0)$, and one solution when $1/h < \psi(\epsilon)$. Let η_1 be the unique point in the range (η_0, ξ_0) such that $\psi(\eta_1) = \psi(\epsilon)$. Let us define

$$h_0 = \frac{1}{\psi(\eta_0)}, \quad h_1 = \frac{1}{\psi(\epsilon)}$$

and denote with $\xi_1(h)$ and $\xi_2(h)$ the two possible solutions to Eq. (21) ($\xi_2(h)$ exists only for $h_0 \leq h \leq h_1$, $\xi_1(h)$ for $h \geq h_0$). In Table 1 we summarize the results about the number of solutions to (21). From (21) it follows also that the two functions $\xi_1(h)$ and $\xi_2(h)$ are monotonic

$$\frac{d\xi_1}{dh} > 0 \quad h \geq h_0, \quad \frac{d\xi_2}{dh} < 0 \quad h_0 \leq h \leq h_1$$

and, moreover, $\lim_{h \rightarrow +\infty} \xi_1(h) = \xi_0$. Let

$$\phi_0 = \phi(\eta_0, h_0), \quad \phi_j(h) = \phi(\xi_j(h), h), \quad j = 1, 2.$$

From the expression of $\partial\phi/\partial x$ and $\psi(x)$ given in (19), we have that $\xi_2(h)$ is a local minimum and $\xi_1(h)$ is a local maximum of $\phi(x, h)$. Since $\xi_2(h) < \xi_1(h)$, it follows that

$$\phi_2(h) < \phi_1(h).$$

Since

$$\frac{\partial\phi}{\partial h} > 0, \quad \left(\frac{\partial\phi}{\partial x}\right)_{x=\xi_j} = 0,$$

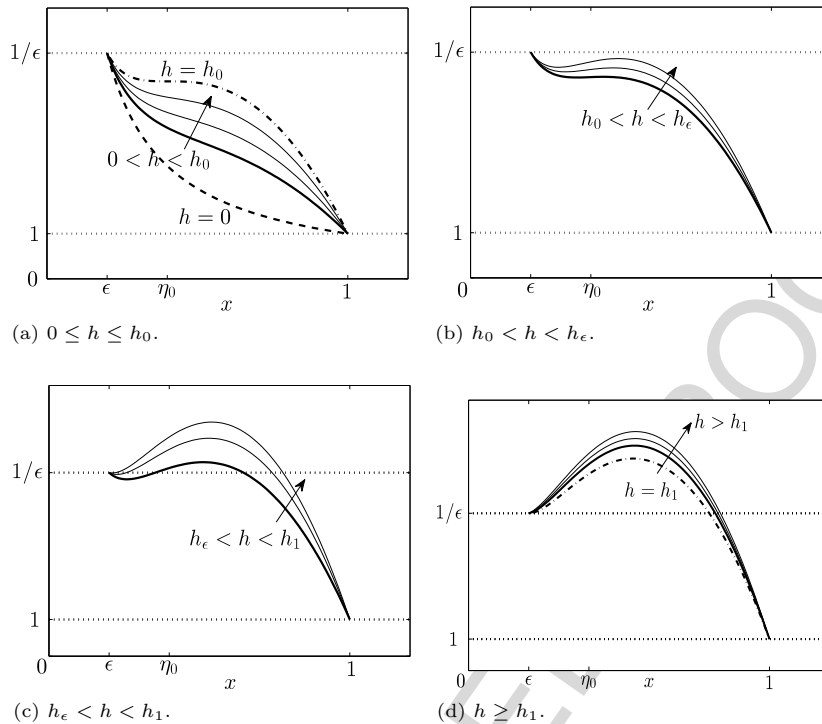


Fig. 2. Trend of $\phi(x, h)$ for $x \in (\epsilon, 1)$ and different values of h . The arrows indicate the direction of increasing h .

from

$$\frac{d\phi_j}{dh} = \left(\frac{\partial \phi}{\partial h} \right)_{x=\xi_j} + \left(\frac{\partial \phi}{\partial x} \right)_{x=\xi_j} \frac{d\xi_j}{dh}$$

it follows that $\phi_j(h)$ are monotonic: $d\phi_j/dh > 0$. Moreover,

$$1 < \phi_0 = \frac{1}{\eta_0} + \beta h_0 g(\eta_0) = \phi_1(h_0) = \phi_2(h_0) < \frac{1}{\epsilon}, \quad \phi_1(h_1) > \phi_2(h_1) = \frac{1}{\epsilon},$$

and

$$\phi_1(h) > \phi(\xi_0, h), \quad \phi_1(h) \rightarrow \phi(\xi_0, h) = \beta h + \frac{1}{\xi_0} \quad \text{as } h \rightarrow +\infty.$$

Lastly, $\phi_1(h)$ may be greater or less than $1/\epsilon$ for $h_0 < h < h_1$. Let h_ϵ be the unique solution to the equation $\phi_1(h) = 1/\epsilon$. Now we are able to plot the qualitative shape of $\phi(x, h)$ for $x \in (\epsilon, 1)$ and different ranges of h (Fig. 2). This figure is representative of the qualitative behaviours of $\phi(x, h)$ (defined in (18)) with $g(x)$ satisfying the properties (4), (6), (7) and (8). The function $\phi(x, h)$, strictly increasing in h , when $0 \leq h < h_0$ (Fig. 2(a)) is strictly decreasing in x ; when $h_0 < h < h_1$ (Fig. 2(b), (c)), it shows a local minimum for x between ϵ and η_0 and a local maximum for x between η_0 and 1; finally, when $h > h_1$ (Fig. 2(d)), $\phi(x, h)$ has only a local maximum.

4.2. Solutions to $\phi(x, h) = p/p_0$

Taking into account the results of the previous subsection, we can determine the ranges of p/p_0 for which we have solutions to (18), with $x \in (\epsilon, 1)$, in the various intervals of the parameter h in which $\phi(x, h)$ shows different trends versus x (Fig. 2). For $0 \leq h < h_0$ we have one solution to (18). For $h_0 < h < h_1$ we may

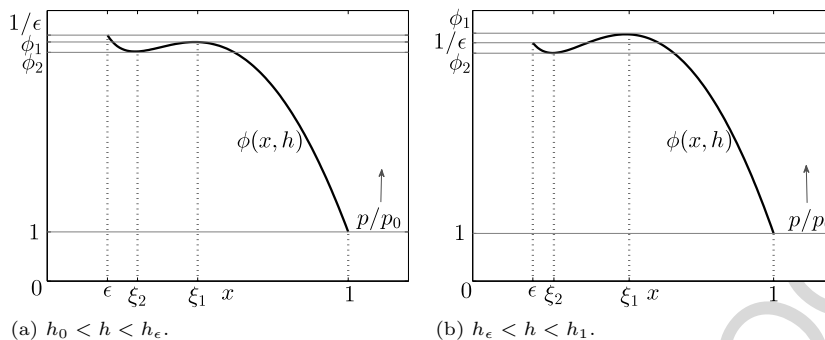


Fig. 3. Solutions to $\phi(x, h) = p/p_0$ for $x \in (\epsilon, 1)$ and $h_0 < h < h_1$.

Table 2

Ranges of p/p_0 for the existence of solutions $x_{*j} = x_{*j}(h, p) \in (\epsilon, 1)$ to Eq. (18), their number, and their positions on the x axis, depending on h ; $\phi_j = \phi_j(h)$, $\xi_j = \xi_j(h)$.

h	p/p_0	Number of solutions to $\phi = p/p_0$	Position on the x axis
$0 \leq h < h_0$	$1 < p/p_0 < 1/\epsilon$	1	$\epsilon < x_{*1} < 1$
$h = h_0$	$1 < p/p_0 < \phi_0$	1	$\eta_0 < x_{*1} < 1$
	$p/p_0 = \phi_0$	1	$\eta_0 = x_{*1} = x_{*2} = x_{*3}$
	$\phi_0 < p/p_0 < 1/\epsilon$	1	$\epsilon < x_{*1} = x_{*3} < \eta_0$
$h_0 < h < h_\epsilon$	$1 < p/p_0 < \phi_2$	1	$\xi_1 < x_{*1} < 1$
	$p/p_0 = \phi_2$	2	$x_{*3} = x_{*2} = \xi_2 < \xi_1 < x_{*1}$
	$\phi_2 < p/p_0 < \phi_1$	3	$\epsilon < x_{*3} < \xi_2 < x_{*2} < \xi_1 < x_{*1} < 1$
	$p/p_0 = \phi_1$	2	$x_{*3} < \xi_2 < x_{*2} = x_{*1} = \xi_1$
	$\phi_1 < p/p_0 < 1/\epsilon$	1	$\epsilon < x_{*3} < \xi_2$
$h_\epsilon < h < h_1$	$1 < p/p_0 < \phi_2$	1	$\xi_1 < x_{*1} < 1$
	$p/p_0 = \phi_2$	2	$x_{*3} = x_{*2} = \xi_2 < \xi_1 < x_{*1}$
	$\phi_2 < p/p_0 < 1/\epsilon$	3	$\epsilon < x_{*3} < \xi_2 < x_{*2} < \xi_1 < x_{*1} < 1$
	$1/\epsilon < p/p_0 < \phi_1$	2	$\xi_2 < x_{*2} < \xi_1 < x_{*1} < 1$
	$p/p_0 = \phi_1$	1	$x_{*2} = x_{*1} = \xi_1$
$h \geq h_1$	$1 < p/p_0 \leq 1/\epsilon$	1	$\xi_1 < x_{*1} < 1$
	$1/\epsilon < p/p_0 \leq \phi_1$	2	$\epsilon < x_{*2} \leq \xi_1 \leq x_{*1} < 1$
	$p/p_0 = \phi_1$	1	$x_{*2} = x_{*1} = \xi_1$

have from one to three solutions; in Fig. 3 we illustrate the positions of the local minimum and maximum of $\phi(x, h)$ with respect to $1/\epsilon$, which determine the regions in the parameter space (h, p) of existence of the solutions to (18). In detail, Fig. 3(a) represents the scenario for $h_0 < h < h_\epsilon$ sketched in Fig. 2(b), where for increasing p from p_0 to p_0/ϵ , $p \neq p_0\phi_i$, $i = 1, 2$, we can have one, three, one equilibria. Fig. 3(b) represents instead the situation for $h_\epsilon < h < h_1$ sketched in Fig. 2(c), where for increasing p from p_0 to $p_0\phi_1$, $p \neq p_0\phi_2$, we can have one, three, two equilibria. For $h > h_1$ we may have one or two solutions to (18) depending on the value of p/p_0 compared to $1/\epsilon$. The results are collected in the following Table 2 and shown in Fig. 4.

In the parameter space (h, p) (Fig. 4) the curves $p = p_0\phi_1(h)$, $h \in (h_0, h_\epsilon)$, and $p = p_0\phi_2(h)$, $h \in (h_0, h_1)$, are stationary bifurcation curves. For $h \in (h_0, h_1)$ and increasing p from p_0 , when $p = p_0\phi_2(h)$ the states E_{*2} and E_{*3} appear, but they do not collide with E_{*1} . Otherwise, when $p = p_0\phi_1(h)$ the states E_{*1} and E_{*2} collide and disappear, but do not collide with E_{*3} . On these curves the determinant of the Jacobian matrix $J(E_{*j}(h, p))$ associated with (3) is zero when evaluated at the colliding equilibria (it will be shown in Section 5). This behaviour is typical of a saddle–node bifurcation. In addition, the two bifurcation curves $p = p_0\phi_1(h)$ and $p = p_0\phi_2(h)$ intersect at the critical point $B_0 = (h_0, p_0\phi_0)$, the unique one in the parameter space where the three equilibrium states coincide. At this point, the two bifurcation curves share a common tangent, since $x_{*j} = \eta_0$, $j = 1, 2, 3$ and, from (20), $\partial\phi_1/\partial h = \partial\phi_2/\partial h = \beta g(\eta_0)$; then B_0 is a mathematical

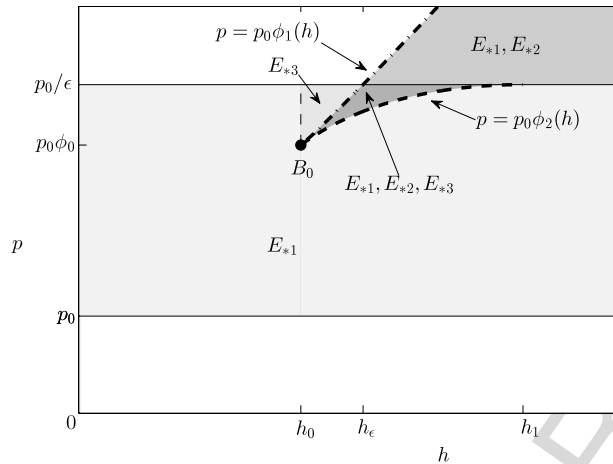


Fig. 4. Existence regions of coexistence equilibrium states in the (h, p) plane, displayed in grey; a different shade denotes a different number of equilibria lying in the region.

cusps in the (h, p) plane. Moreover, we notice that at point B_0 we have, from (19),

$$\frac{\partial \phi}{\partial x}(x_{*j}, h_0) = 0 \quad \text{and} \quad \frac{\partial^2 \phi}{\partial x^2}(x_{*j}, h_0) = 0.$$

All these results indicate the presence of a cusp singularity, according to the Whitney’s theory [33], for the equilibrium surface $p = p_0\phi(x, h)$; the level sets of such surface in the (x, p) plane for fixed h can be deduced from Fig. 2.

In the (h, p) plane the lines

$$\frac{p}{p_0} = 1, \quad \frac{p}{p_0} = \frac{1}{\epsilon}, \quad \frac{p}{p_0} = \phi_j(h), \quad j = 1, 2$$

are boundary lines of existence regions (Fig. 4) for the coexistence equilibrium states $E_{*j}(h, p) = (x_{*j}(h, p), y_{*j}(h, p))$.

For $x_{*j} \neq \xi_1(h), \xi_2(h)$, from Eq. (18) it follows that

$$\frac{\partial x_{*j}}{\partial h} = -\beta g(x_{*j}) \left(\frac{\partial \phi}{\partial x} \right)^{-1}_{x_{*j}}, \quad \frac{\partial x_{*j}}{\partial p} = \left(p_0 \frac{\partial \phi}{\partial x} \right)^{-1}_{x_{*j}}.$$

Since $(\partial \phi / \partial x)$ is negative for $x = x_{*1}, x_{*3}$ and positive for $x = x_{*2}$, we have the following monotonicity properties for x_{*j} :

$$\frac{\partial x_{*1}}{\partial h} > 0, \quad \frac{\partial x_{*j}}{\partial p} < 0, \quad j = 1, 3; \quad \frac{\partial x_{*2}}{\partial h} < 0, \quad \frac{\partial x_{*2}}{\partial p} > 0.$$

The bifurcation process is described in detail in the bifurcation diagrams (Fig. 5), where x_{*j} are reported versus p for different values of h , corresponding to the four different ranges of h of Fig. 2. With reference also to Fig. 4, we can see in detail in Fig. 5 how the equilibrium states collide and disappear. In all subplots transcritical bifurcation points, marked with BP, are located on the lines $p = p_0$ and $p = p_0/\epsilon$ of Fig. 4; saddle–node bifurcation points (LP) lie on the curves $p = p_0\phi_1(h)$ and $p = p_0\phi_2(h)$.

The coexistence equilibrium states, when they exist, lie on the curve $y = \beta x g(x)$, $x \in (\epsilon, 1)$, in the phase space. Obviously, their number and their position depend on the parameters h and p , and their behaviour is determined by the trends of $x_{*j}(h, p)$, $j = 1, 2, 3$, versus h and p .

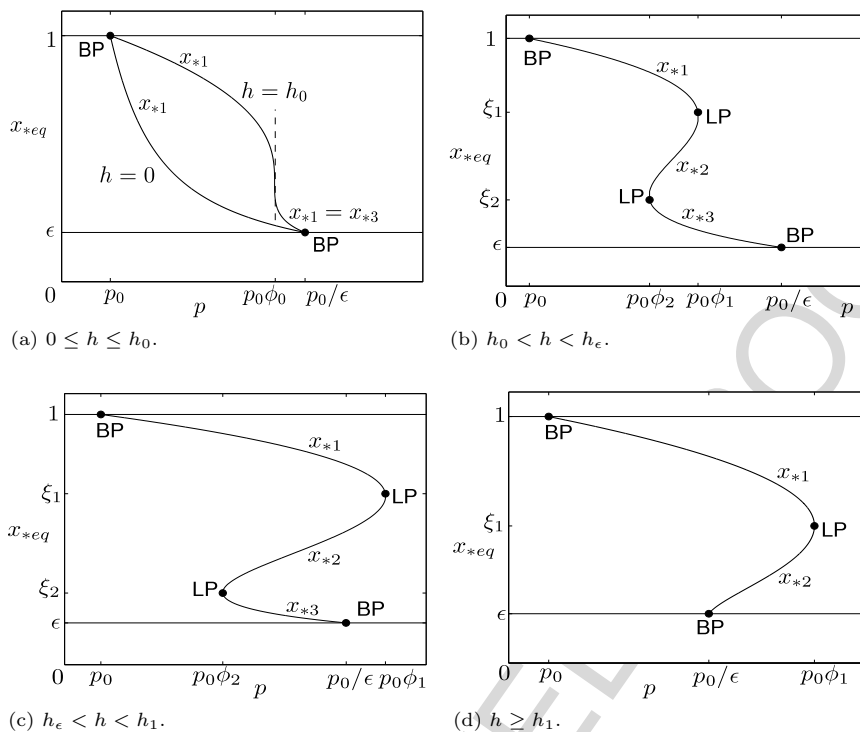


Fig. 5. Qualitative trend of x_{*j} versus p for different values of h . BP: transcritical bifurcation, LP: saddle–node bifurcation.

Remark. (IV) On the boundary line $h = h_0$, $p \in (p_0\phi_0, p_0/\epsilon)$ (Fig. 4) the determinant of $J(E_{*1}(h, p))$ is positive (see Section 5), and therefore it is not a local bifurcation line. On this line, the trend of x_{*1} versus p is reported in Fig. 5(a) and shows an inflection point with vertical tangent at $p = p_0\phi_0$. When $p_0\phi_0 < p < p_0/\epsilon$, we have that

$$\lim_{h \rightarrow h_0^+} E_{*3}(h, p) = \lim_{h \rightarrow h_0^-} E_{*1}(h, p),$$

namely the equilibria swap names; this line has been introduced in order to allow a smooth transition of the equilibrium E_{*3} , instead of an abrupt change from E_{*3} to E_{*1} , on the bifurcation line $p = p_0\phi_1$ (see Fig. 5(b)).

5. Stability properties of coexistence equilibrium states

Let $E_*(h, p) = (x_*(h, p), y_*(h, p))$ be a generic coexistence equilibrium state. From the expression of the Jacobian matrix displayed in Section 3, and taking into account the relations satisfied by $x_*(h, p)$ and $y_*(h, p)$, we may write the Jacobian matrix associated with $E_*(h, p)$ in the form

$$J(E_*(p, h)) = r_x \begin{pmatrix} (1 - \mu_0)g(x_*) + x_*g'(x_*) & -1/\beta + \mu_0g(x_*)hp_0/p \\ c\mu_0g(x_*) & -c\mu_0g(x_*)hp_0/p \end{pmatrix}$$

with $x_* = x_*(h, p)$, and

$$\mu_0 = \mu(p_0), \quad 0 < \mu_0 < 1,$$

where $\mu(s) = sf'(s)/f(s)$; its properties are discussed in [Appendix B](#). Let

$$D(h, p, x_*) = \text{Det } J(E_*(h, p)), \quad T(h, p, x_*) = \text{Tr } J(E_*(h, p)).$$

By direct computation, and taking into account [\(18\)](#) and [\(19\)](#), we obtain

$$D(h, p, x_*) = -\frac{r_x m \mu_0 p_0 g(x_*)}{p x_*} [-1 + h \beta x_*^2 g'(x_*)] = -\frac{r_x m \mu_0 p_0 g(x_*) x_*}{p} \left(\frac{\partial \phi}{\partial x} \right)_{x=x_*},$$

$$T(h, p, x_*) = r_x (\Lambda(h, p) g(x_*) + x_* g'(x_*)),$$

where

$$\Lambda(h, p) = 1 - \mu_0 - c \mu_0 h \frac{p_0}{p}.$$

Since $(\partial \phi / \partial x)_{x=x_*} > 0$, it follows that $\text{Det } J(E_{*2}(h, p)) < 0$ for h and p not belonging to the bifurcation curves of [Fig. 4](#); thus, $E_{*2}(h, p)$ is a saddle point. Otherwise, for $j = 1, 3$, since $(\partial \phi / \partial x)_{x=x_{*j}} < 0$, it follows that $\text{Det } J(E_{*j}(h, p)) > 0$, for h and p not belonging to bifurcation curves; thus, $E_{*j}(h, p)$, $j = 1, 3$, is locally asymptotically stable iff $T(h, p, x_{*j}) < 0$. Here we summarize the main stability results obtained for the states $E_{*1}(h, p)$ and $E_{*3}(h, p)$. Technical details and some remarks are reported in [Appendix C](#).

As regards the equilibrium $E_{*1}(h, p)$, an important role for its stability properties is played by the two implications

$$\Lambda(h, p) \leq 0 \iff \frac{p}{p_0} \leq \gamma h; \quad (22)$$

$$x_{*1}(h, p) \geq \xi_0 \iff \frac{p}{p_0} \leq \phi(\xi_0, h) = \beta h + \frac{1}{\xi_0}, \quad (23)$$

where

$$\gamma = \frac{c \mu_0}{1 - \mu_0}. \quad (24)$$

Two scenarios emerge, depending on the intersection of the two straight lines

$$\frac{p}{p_0} = \gamma h, \quad \frac{p}{p_0} = \beta h + \frac{1}{\xi_0}$$

in the (h, p) plane; the intersection occurs when $\beta < \gamma$, i.e. when

$$r_x < r_0 = \frac{m \mu_0}{1 - \mu_0}. \quad (25)$$

5.1. State E_{*1} : the case of $r_x \geq r_0$

Under the assumption $r_x \geq r_0$, or equivalently $\beta \geq \gamma$, we have that in the (h, p) plane

$$\beta h + \frac{1}{\xi_0} > \gamma h \quad \forall h > 0.$$

We refer to [Fig. 6](#) to illustrate the results of this case.

There exists a curve $p = p_1(h)$ (see [Theorem 2](#) and its proof in [Appendix C](#)) on which $\text{Tr } J(E_{*1}(h, p_1(h))) = 0$; this curve is monotonically increasing and

$$p_0 \max\{1, \gamma h\} < p_1(h) < p_0 \left(\beta h + \frac{1}{\xi_0} \right).$$

For all the considered functions $g(\cdot)$ and $f(\cdot)$ in [\(10\)–\(13\)](#) and the parameter values specified in [Appendix B](#), $p_1(h)$ turns out to be very close to $\beta h + 1/\xi_0$. The existence region of $E_{*1}(h, p)$ in the (h, p) plane is divided in three subregions ([Fig. 6](#)): the white regions [\[1\]](#) and [\[2\]](#), where $E_{*1}(h, p)$ is locally stable, and the grey region [\[3\]](#), where it is unstable.

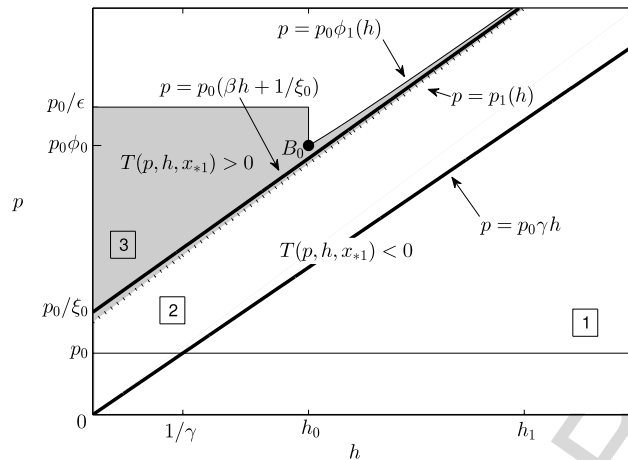


Fig. 6. Local stability and instability regions in the (h, p) plane of the coexistence equilibrium state $E_{*1}(h, p)$ in the case $r_x \geq r_0$. In grey the region in which $T(h, p, x_{*1}) > 0$.

Let $\Delta(h, p, x_{*1}) = T^2(h, p, x_{*1}) - 4D(h, p, x_{*1})$. For fixed $h \geq 0$, at $p = p_1(h)$ we have

$$T(h, p_1(h), x_{*1}(h, p_1(h))) = 0, \quad \Delta(h, p_1(h), x_{*1}(h, p_1(h))) < 0,$$

so that the Jacobian matrix has a simple pair of pure imaginary eigenvalues. Moreover, $dT/dp > 0$ for $\max\{1, \gamma h\} < p/p_0 < \beta h + 1/\xi_0$. Thus, $p = p_1(h)$ is a Hopf bifurcation curve for the equilibrium $E_{*1}(h, p)$ (the dotted one in Fig. 6), and limit cycles emerge for p in a neighbourhood of $p_1(h)$. The stability of the limit cycles can be determined by the sign of the first Lyapunov coefficient associated with the system (3) ([34] p. 152, formula (3.4.11); [35] p. 178, formula (5.62)) once the model functions are fixed. The dependence of this coefficient on the parameters h and p is very intricate, and a theoretical analysis is a substantial undertaking. The sign was then determined numerically (and also checked with the specific software MATCONT [36]) for special systems characterized by different prey growth and trophic functions, and the set of bioecological parameters given in Appendix B; also the side of the Hopf bifurcation curve on which the limit cycles exist has been found numerically. The results will be illustrated in the next section.

5.2. State E_{*1} : the case of $r_x < r_0$

The situation is somewhat more involved than in the previous case. We refer to Fig. 7 to illustrate the results of this case. Under the assumption $r_x < r_0$, or equivalently $\beta < \gamma$, we have that in the (h, p) plane the line $p/p_0 = \gamma h$ intersects the line $p/p_0 = \beta h + 1/\xi_0$ and the curve $p = p_0\phi_1(h)$ at points R and S , respectively. Let h_R (independent of p) and h_S (dependent on p) be the h -coordinates of the intersection points R and S ; we have

$$h_R = \frac{1}{\xi_0(\gamma - \beta)} = \frac{1}{\xi_0\beta(r_0/r_x - 1)}, \quad h_S = \phi_1^{-1}\left(\frac{p}{p_0}\right). \quad (26)$$

There exists a Hopf bifurcation curve $p = p_1(h)$ for $h < h_R$ (see Theorem 3 in Appendix C) which is monotonically increasing (Fig. 7). Also in this case, the stability of the limit cycles has been numerically studied and the results will be discussed in the next section.

In general, the stability properties of $E_{*1}(h, p)$ cannot be established in the subregion of existence (marked with dark grey in Fig. 7(b)) defined by

$$h > h_R, \quad \beta h + \frac{1}{\xi_0} < \frac{p}{p_0} < \min\{\gamma h, \phi_1(h)\}. \quad (27)$$

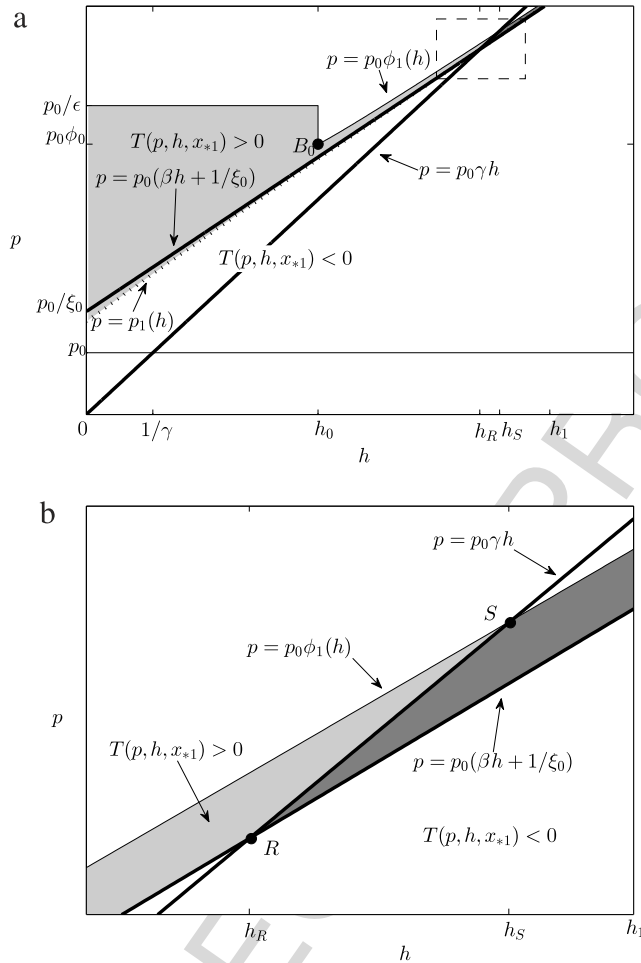


Fig. 7. Local stability and instability regions in the (h, p) plane of the coexistence equilibrium state $E_{*1}(h, p)$ in the case $r_x < r_0$. Light grey denotes regions in which $T(p, h, x_{*1}) > 0$; dark grey marks regions in which the stability properties of E_{*1} cannot be analytically determined. Figure (b) is an enlargement of the dashed rectangular region of figure (a).

Indeed, in this region the implications (22) and (23) do not hold and we have no information about the sign of $T(h, p, x_{*1})$. It is possible nevertheless to check the sign of the trace $T(h, p, x_{*1})$ along the curve $p = p_0\phi_1(h)$ and it turns out that for h slightly above h_S $T(h, p, x_{*1}) > 0$ and $\lim_{h \rightarrow +\infty} T(h, p, x_{*1}) = r_x(1 - \mu_0)(1 - \gamma/\beta)$. Such value is negative only when $r_x < r_0$ and then, thanks to the monotonicity properties (C.1) (see Appendix C), there exists a unique value h_{BT} wherein $T(h_{BT}, p, x_{*1}) = 0$. These facts reveal the presence of a Bogdanov–Takens point, intersection of a saddle–node, a Hopf and a separatrix homoclinic loop curve, that will be discussed in the next section.

5.3. State E_{*3}

From the existence conditions of $E_{*3}(p, h)$ and implication (22) it follows that for $h_0 \leq h \leq h_1$ we have

$$\max \{ \phi_2(h), \gamma h \} < \frac{p}{p_0} < \frac{1}{\epsilon} \implies T(p, h, x_{*3}) > 0.$$

The situation for E_{*3} is illustrated in Fig. 8. Let $\tilde{h}_1 = 1/(\gamma\epsilon)$ be the intersection point between the straight lines $p = p_0/\epsilon$ and $p = p_0\gamma h$.

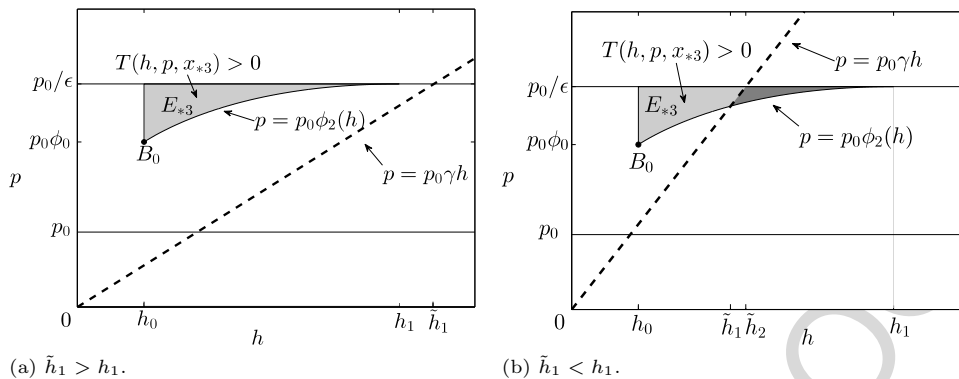


Fig. 8. Instability regions in the (h, p) plane of the coexistence equilibrium state $E_{*3}(h, p)$.

If

$$\tilde{h}_1 \geq h_1, \quad \text{i.e. } \frac{r_0}{r_x} \leq \epsilon g'(\epsilon),$$

then $E_{*3}(p, h)$ is unconditionally unstable (Fig. 8(a)). For instance, this case holds for a Holling-type II trophic function, a Gilpin model for $g(s)$ and parameters as in Appendix B with $r_x > r_0$.

If

$$\tilde{h}_1 < h_1, \quad \text{i.e. } \frac{r_0}{r_x} > \epsilon g'(\epsilon),$$

then, in general, the stability properties of $E_{*3}(h, p)$ cannot be established in the region defined by

$$\tilde{h}_2 \leq h \leq h_1, \quad \phi_2(h) \leq \frac{p}{p_0} \leq \min \left\{ \gamma h, \frac{1}{\epsilon} \right\},$$

where \tilde{h}_2 is the unique solution to the equation $\gamma h = \phi_2(h)$ (dark grey region in Fig. 8(b)). Indeed, in this region the implication (22) does not hold and we have no information about the sign of $T(h, p, x_{*3})$.

The stability properties of all equilibrium states are summarized in Table 3.

Q5

6. Behaviours of the system

Here we focus on some peculiar behaviours obtained by using the model functions (10)–(13), and the parameter values specified in Appendix B. Such behaviours are of course in agreement with the analytical results obtained in the previous sections. Once the model functions are fixed, we can also numerically investigate the limit cycles arising from E_{*1} by Hopf bifurcation. The main features of the bifurcation structure will be shown in the following diagrams, which are only qualitative because the real bifurcation curves, simulated here by using model functions (10) and (12) and parameter values as in Appendix B, are almost indistinguishable from one another. Therefore, some of the phenomena described below can be viewed only with a very fine resolution. Anyhow, we obtain qualitatively the same scenarios with different combinations of model functions (10)–(13). Further information on the bifurcation structure close to critical values of the bifurcation parameters detected in the following analysis (such as number of bifurcating limit cycles, higher codimension points, ...) could be obtained case by case with specific model functions and it will be matter of a future work.

- When $0 < h < h_0$, in all tested cases, independently of the value of r_x , the numerical results showed the existence of a critical value \hat{h} such that:

Table 3
 (a) Summary of stability properties of equilibrium states (n.d. = not determinable, unst. = unstable); (b) details on stability of $E_{*1}(h, p)$ for $h_0 < h < h_1$ and $r_x < r_0$.

	$0 \leq h \leq h_0$	$h_0 < h < h_1$	$h > h_1$
(a)			
E_0	stable node $p > 0$		
E_ϵ	saddle $0 < p < p_0/\epsilon$, unst. node $p > p_0/\epsilon$		
E_1	stable node $0 < p < p_0$, saddle $p > p_0$		
$E_{*1}(h, p)$	stable $p_0 < p < p_1(h)$ unst. $p_1(h) < p < p_0/\epsilon$	$r_x \geq r_0$ stable $p_0 < p < p_1(h)$ unst. $p_1(h) < p < p_0\phi_1(h)$ see Table 3(b)	stable $p_0 < p < p_0(\beta h + 1/\xi_0)$ n.d. $p_0(\beta h + 1/\xi_0) < p < p_0\phi_1(h)$
$E_{*2}(h, p)$	#	saddle $p_0\phi_2(h) \leq p \leq p_0\phi_1(h)$	saddle $p_0/\epsilon \leq p \leq p_0\phi_1(h)$
$E_{*3}(h, p)$	#	unst. $\max\{p_0\phi_2(h), p_0\gamma h\} \leq p \leq p_0/\epsilon, h_0 < h < \tilde{h}_1$ n.d. $p_0\phi_2(h) \leq p \leq \min\{p_0\gamma h, p_0/\epsilon\}, \tilde{h}_2 < h < h_1$	#
(b)			
$E_{*1}(h, p)$ ($r_x < r_0, h_0 < h < h_1$)	$h_0 < h < h_R$ stable $p_0 < p < p_1(h)$ unst. $p_1(h) < p < p_0\phi_1(h)$	$h_R < h < h_S$ stable $p_0 < p < p_0(\beta h + 1/\xi_0)$ n.d. $p_0(\beta h + 1/\xi_0) < p < p_0\gamma h$ unst. $p_0\gamma h < p < p_0\phi_1(h)$	$h_S < h < h_1$ stable $p_0 < p < p_0(\beta h + 1/\xi_0)$ n.d. $p_0(\beta h + 1/\xi_0) < p < p_0\phi_1(h)$

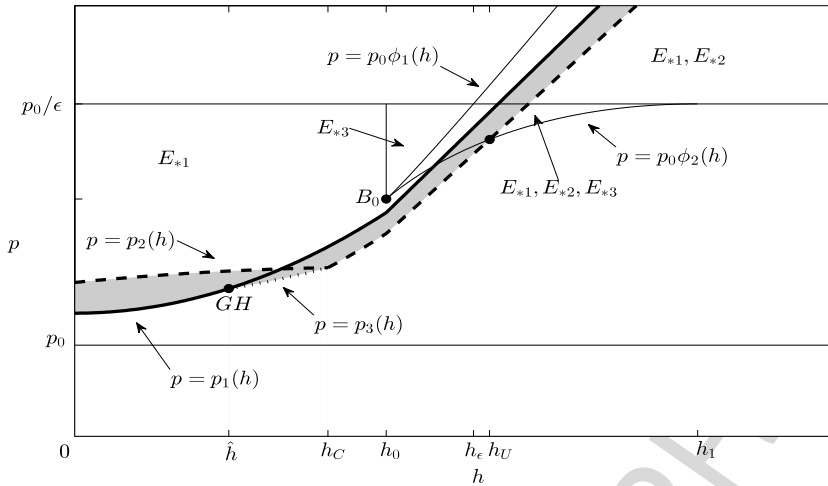


Fig. 9. Qualitative representation of local and global bifurcation curves for the equilibrium E_{*1} and limit cycles; in grey the regions of the (h, p) plane in which stable or unstable limit cycles exist. GH: Generalized Hopf point.

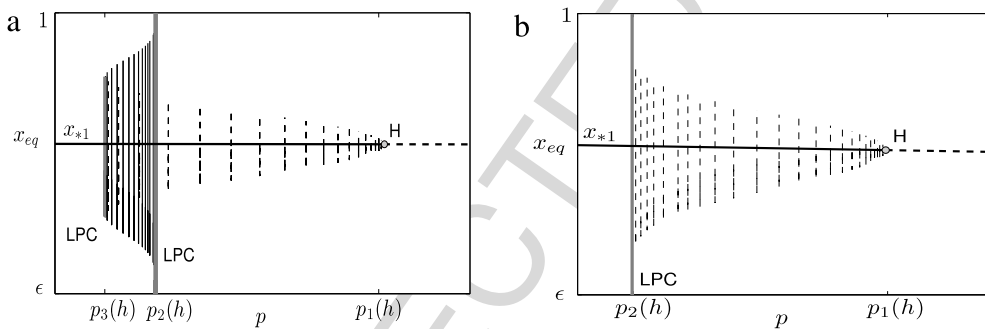


Fig. 10. Limit cycles behaviours versus p . (a) $\hat{h} < h < h_C$, \hat{h} close to h_C (for h slightly greater than \hat{h} the Hopf point $p_1(h)$ is instead between $p_3(h)$ and $p_2(h)$); (b) $h_C < h < h_0$; the vertical lines represent the projections of the limit cycles on the (p, x) plane. Solid lines: stable cycles, dashed lines: unstable cycles. LPC denotes bifurcation of limit cycles detected by MATCONT, while H indicates a Hopf point.

- for any fixed $0 \leq h < \hat{h}$, stable limit cycles emerge for p slightly above the Hopf value $p_1(h)$ and disappear by global bifurcation with the heteroclinic cycle involving equilibria E_ϵ and E_1 at a further critical value $p_2(h) > p_1(h)$ (see Fig. 9); in this range of h the system behaves qualitatively as the system with $h = 0$ [12, Figure 7];
- when $h > \hat{h}$, repelling limit cycles emerge for p slightly below the Hopf value $p_1(h)$. We have numerical evidence of the existence of a further critical value h_C such that for $\hat{h} < h < h_C$ (Fig. 9) the repelling limit cycles disappear by saddle–node bifurcation with a stable limit cycle on the curve $p = p_3(h)$, and stable limit cycles then disappear by global bifurcation involving the heteroclinic cycle between equilibria E_ϵ and E_1 (Fig. 10(a)) on the curve $p = p_2(h)$ (Fig. 9). The curve of heteroclinic cycles $p = p_2(h)$ intersects $p = p_3(h)$ for $h = h_C$, while it crosses the Hopf curve $p = p_1(h)$ for a value $h \in (\hat{h}, h_C)$. For $h_C < h < h_0$, the repelling limit cycles disappear instead by global bifurcation with the heteroclinic cycle involving E_ϵ and E_1 (Fig. 10(b)) on the curve $p = p_2(h) < p_1(h)$.

The Hopf bifurcation is thus supercritical for $h < \hat{h}$, and subcritical for $h > \hat{h}$; the curve $p = p_3(h)$ of saddle–node bifurcation of limit cycles emanates from the point $(\hat{h}, p_1(\hat{h}))$. It is possible to detect, by using the continuation software MATCONT [36], that the Hopf bifurcation curve has a Generalized Hopf (GH) codimension-two point at $h = \hat{h}$. A deeper investigation of the bifurcation occurring at $h = h_C$,

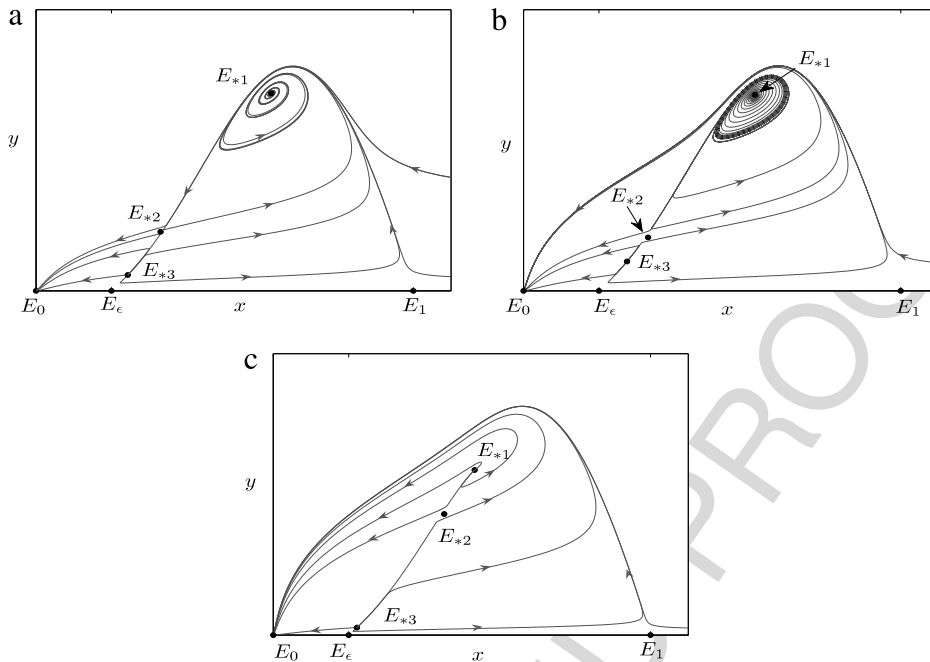


Fig. 11. Phase portraits for $h_0 < h < h_1$ and different p : (a) $p < p_2(h)$, (b) $p_2(h) < p < p_1(h)$, (c) $p > p_1(h)$.

where $p = p_2(h)$ and $p = p_3(h)$ intersect each other, could be performed case by case following [37], with specific model functions, and would allow to determine how many cycles bifurcate in this region of the parameter space and what is their stability; this analysis will be matter of future studies.

- When $h_0 < h < h_1$, again whatever r_x , we have that the coexistence region of the equilibria E_{*1} , E_{*2} , E_{*3} (dark grey region in Fig. 4) is crossed by the Hopf bifurcation curve $p = p_1(h)$ (see Fig. 9). Again, the Hopf bifurcation curve generates unstable limit cycles for p slightly below the Hopf value $p_1(h)$; such cycles disappear by global bifurcation on the curve $p = p_2(h)$, which can occur either with the heteroclinic cycle connecting E_ϵ and E_1 or with a homoclinic cycle with the saddle point E_{*2} . In detail, let h_U be the abscissa of the intersection of the curves $p = p_2(h)$ and $p = p_0\phi_2(h)$ (Fig. 9); then, the heteroclinic cycle occurs for $h < h_U$ and the homoclinic cycle for $h > h_U$. The transition from having heteroclinic to homoclinic orbits turns out to be caused by the formation at $h = h_U$ of a heteroclinic cycle connecting the just appeared equilibrium $E_{*2} = E_{*3}$ and E_1 . This leads to the interaction of the limit cycles with the equilibrium E_{*2} and then to their disappearance by global bifurcation with a homoclinic cycle through E_{*2} , instead of by a heteroclinic cycle connecting E_ϵ and E_1 . The point $h = h_U$ seems to be a codimension-three or even higher bifurcation point. Anyway, a deeper analysis aiming at detecting all possible non equivalent phase portraits around this point cannot be carried out in general and it will be matter of future investigations with specific model functions.

Some examples of the peculiar dynamics obtained for different p and $h_0 < h < h_1$ are reported in the phase portraits in Fig. 11. We selected cases in which all coexistence equilibria are present and we focused on bistability occurring in the system. In Fig. 11(a) (where $p < p_2(h)$) the trajectories tend to E_0 or E_{*1} depending on the initial conditions. In Fig. 11(b) (where $p_2(h) < p < p_1(h)$) an unstable limit cycle separates the basins of attraction of the stable equilibria E_{*1} and E_0 . Lastly, in Fig. 11(c) (where $p > p_1(h)$) all the coexistence equilibria are unstable and the system evolves towards global extinction.

- For $h > h_1$ and $r_x \geq r_0$ we have proved in Theorem 2 (Appendix C) that the Hopf bifurcation curve $p = p_1(h)$ is always below the stationary bifurcation curve $p = p_0\phi_1(h)$ (Fig. 6). The numerical

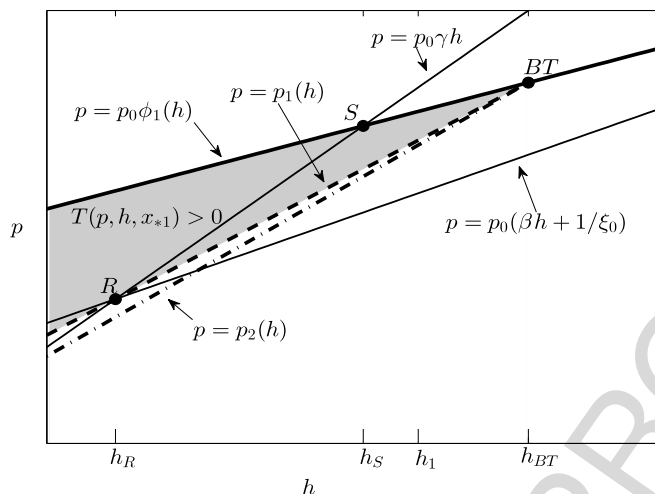


Fig. 12. Qualitative representation of local and global bifurcation curves for the equilibrium E_{*1} and limit cycles for $h > h_R$ in the case $r_x < r_0$. Light grey denotes the region in which $T(h, p, x_{*1}) > 0$. BT: Bogdanov–Takens point.

investigation shows that unstable limit cycles arise below the curve $p = p_1(h)$ and disappear by global bifurcation with a homoclinic cycle through the saddle point E_{*2} on the curve $p = p_2(h) < p_1(h)$.

For $h > h_1$ and $r_x < r_0$, we cannot state in general the mutual positions of the curves $p = p_1(h)$, $p = p_0\phi_1(h)$. Moreover, the stability properties of E_{*1} cannot be determined in general in the region defined in (27) (dark grey region in Fig. 7(b)). We have numerically detected Hopf bifurcation values $p_1(h)$ for E_{*1} also when h is above the estimated threshold h_R (see Fig. 12). Again, unstable limit cycles arise below the curve $p = p_1(h)$ and disappear by global bifurcation with the homoclinic cycle through E_{*2} on the curve $p = p_2(h) < p_1(h)$. The Hopf bifurcation curve $p = p_1(h)$ lies below the line $p = p_0(\beta h + 1/\xi_0)$ for $h < h_R$, intersects it for $h = h_R$ at point R (where $\gamma h = \beta h + 1/\xi_0$) and stays definitely above for $h > h_R$. Since the sign of the trace $T(h, p, x_{*1})$ along the curve $p = p_0\phi_1(h)$ changes from positive to negative, as pointed out in Section 5.2, there exists the critical value $h_{BT} > h_1$ at which the Hopf curve $p = p_1(h)$ intersects the curve $p = p_0\phi_1(h)$. Also the global bifurcation curve $p = p_2(h)$, which involves the homoclinic cycle through the saddle point E_{*2} , passes through this intersection and then we obtain a codimension-two point in the (h, p) plane in which $D(h_{BT}, p_{BT}, x_{*1}) = 0$ and $T(h_{BT}, p_{BT}, x_{*1}) = 0$, that turns out to be a Bogdanov–Takens (BT) bifurcation point. It is characterized by the typical phase diagram of Fig. 13; this type of bifurcation has been detected by other authors in similar models [38–41].

7. Concluding remarks

When modelling predator–prey systems, the properties of the prey growth function $g(\cdot)$ depend on the introduction of intraspecific competition among the prey, and on the assumption of either the absence or the presence of a weak/strong Allee effect. On the other hand, the trophic function $f(\cdot)$ may be assumed either concave or S-shaped and it can be prey-dependent, ratio-dependent or predator–prey dependent. Moreover, only some of their qualitative properties are known. Thus, these functions should not be specified by any analytical expression, but only by general properties dictated by bioecological considerations; moreover, they should satisfy some technical assumptions to make the analysis tractable.

The assumptions made on the model functions limit the number of equilibrium points, and allow to perform a sufficiently general existence, stability and bifurcation analysis of the equilibrium states. However, this approach leads to some restrictions in the analysis of the dynamics. Let us look at the assumptions

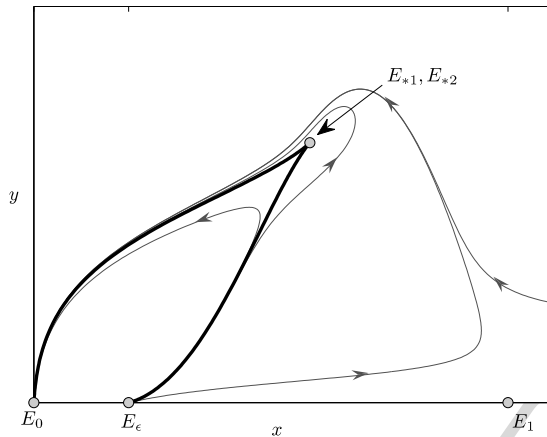


Fig. 13. Phase diagram close to the Bogdanov–Takens bifurcation $h = h_{BT}$, $p = p_{BT}$.

(4)–(9) on g and f in this paper. These conditions imply relationships between $f(s)$, $f'(s)$ and $g(s)$, $g'(s)$, $g''(s)$. At any rate, when a Hopf bifurcation is detected, the stability properties of the limit cycles cannot be in general established from the sign of the first Lyapunov number, because it depends on the first, second and third derivatives of the right hand side of (3), evaluated at the equilibrium point. In the very recent paper by Adamson and Morozov [42] it is pointed out that “the use of two different functions belonging to the same class can result in qualitatively different dynamical behaviour in the model and a different type of bifurcation. In the literature, the conventional way to avoid such ambiguity is to narrow the class of unknown functions”, and they conclude that this approach may lead to cumbersome expressions, biologically meaningful. We observe that some uncertainties could be removed by carrying out many numerical simulations with different model functions.

In our approach, the use of different functions belonging to the same class leads to some common behaviours, for instance in connection with the number of equilibria and their stability properties. However, some peculiar dynamics, such as the phase diagram close to the Bogdanov–Takens bifurcation point in the case of $r_x < r_0$, can be found only with specific functions in the class. Adamson and Morozov [42] analyse in detail this crucial problem and show that where the model functions are not specified by analytical expressions, the bifurcations can be described only with a certain probability.

We wish to point out that slightly different formulations of the model equations, together with rescaling of state variables and parameters and the use of different bifurcation parameters in the stability analysis, lead to hard-working comparison between the various scenarios. In any event, behaviours of predator–prey systems of type (3) characterized by different model functions $g(\cdot)$ and $f(\cdot)$ analysed in the literature [13,43,40,38,41,44,45,39,12], deserve some attention. Under the assumption of a strong Allee effect, the functions implemented in the aforementioned literature, and combined in different ways in system (3), are (10)–(13).

In the case of a prey-dependent trophic function, realized by setting $h = 0$ in (3), comparisons of models characterized by combinations of (10)–(11) and (12)–(13) have been reported in [12]. The existence and stability analysis of the equilibrium states had been performed by taking p and the ratio $\theta = m/(cb)$ as bifurcation parameters. All the considered models admit the same equilibrium states, and show the same qualitative behaviours regarding the local stability properties, the occurrence of a heteroclinic cycle and the consequent global bifurcation. Obviously, the stability ranges may be very different, with the same values of the bioecological parameters r_x , b , m , c .

Also the model in the recent paper [44], with an Allee effect of rational type $g(s) = g_0(s - \epsilon)(1 - s)/(\epsilon_0 + s)$ with $\epsilon_0 > 0$ (called double Allee effect) and linear trophic function $f(s) = s$ (Lotka–Volterra interaction) undergoes a heteroclinic loop bifurcation, and moreover subcritical and supercritical Hopf bifurcation.

In all the visited models with Allee effect and prey-dependent trophic function it has been observed only one possible coexistence state, which may experiment different histories. For instance, assuming ϵ_0 in the double Allee effect as bifurcation parameter, the coexistence equilibrium state can switch from stable to unstable and then back again to stable [46,44].

The ratio-dependent trophic function expressed in terms of the ratio $x/(x+y)$, which is singular in the origin, has been recently introduced in models with Allee effect of quadratic type (Gilpin model (10)) in [39,41,38], and of rational type (double Allee effect) in [40]. In all these models only two coexistence states may be found, and one is always a saddle point. In the different parameter spaces considered by these authors, a Bogdanov–Takens bifurcation point of codimension-two has been detected and it is considered “as an organizing centre of the global dynamics” [38]. Although these models have the same structure, the analysis and the numerical simulations performed in [39,41] show and suggest the absence of stable limit cycles, while in [38] “for a fixed set of parameters, the following may happen: the extinction of both populations, coexistence for determined population sizes, or the oscillation of both population”. The same results are obtained in [40]. A possible explanation is the following: in [38,40] a parameter introduced in the prey growth function, associated with ϵ in our formulation, is used as bifurcation parameter, and varied in the numerical simulations, while it is maintained fixed in [39]. Furthermore, in [38,40] more global phenomena are described: heteroclinic loop and bifurcation of limit cycles. The results obtained in [46,44,38,40] suggest that the use of parameters introduced in the prey growth function as a bifurcation parameter put in evidence phenomena which are not detected by performing the analysis with other bifurcation parameters.

In our analysis, we fixed all the dimensional bioecological rates r_x , b , m , determining the time scale of the dynamics and the conversion factor c from prey to predator biomass, which are multiplicative factors in Eq. (3). Moreover, also the Allee threshold ϵ is maintained fixed. The parameters h and p appearing in the argument of the trophic function, which describes the predator–prey interaction, have been chosen as bifurcation parameters. In our analytical study, we found that the system admits at most three coexistence equilibria E_{*1} , E_{*2} , E_{*3} depending on the values of parameters h and p , as in Table 2. The coexistence equilibrium E_{*2} , when exists, is always a saddle point. The equilibrium E_{*3} is always unstable when the straight line $p = p_0\gamma h$ does not intersect its existence region in the (h, p) plane.

The study of the stability properties of E_{*1} in the (h, p) plane is more intricate. We found a Hopf bifurcation curve $p = p_1(h)$, and limit cycles emerge, stable or unstable depending on the value of h , and disappear by global bifurcation, involving the heteroclinic cycle between the non coexistence equilibria E_ϵ , E_1 or the homoclinic cycle through the coexistence equilibrium E_{*2} , respectively. Furthermore, we have also numerically detected a region in the (h, p) plane where stable and unstable limit cycles coexist and disappear by saddle–node bifurcation of cycles. Finally, we proved the existence of a Bogdanov–Takens bifurcation point for $r_x < r_0$. We pointed out that, in some regions of the parameter space, the model presents multiple attractors. Moreover, the extinction of both populations is always possible, since the global extinction E_0 is always locally asymptotically stable and globally stable for some parameter values.

A last brief remark concerns the maximal specific production rates r_x and r_y . A critical value r_0 , defined in (25), of r_x was found. It depends on the bioecological parameters b , m , c and on the type of the trophic function. The behaviour of the system shows different features depending on the sign of the difference $r_x - r_0$. This fact is independent of either the presence or the absence of an Allee effect in the model equations (see Sections 5.1 and 5.2 and [12]). It is worthwhile noting that the difference in the system behaviour due to the sign of $r_x - r_0$ becomes very marked when a trophic function singular in the origin is used [47]. Furthermore, it can be observed (see Appendix C) that with a Holling-type II trophic function we have $r_0 = r_y$, while with an Ivlev type $r_0 > r_y$ with the same bioecological parameters m , c , b . Thus, if $r_x < r_y$, then $r_x < r_0$, with a Holling-type II trophic function. Contrarily, with the Ivlev trophic function, when $r_x > r_y$ we might have either $r_x < r_0$ or $r_x > r_0$. We recall that, in general, in a food web the time needed for reproduction

and growth of the individuals of a population is increasing with the trophic level [48,47]. At any event, in some predator–prey systems, such as some acarine systems, any situation may occur.

Summarizing, the general approach to predator–prey systems used in this paper, in which the mathematical formulation of model functions is unspecified except for some generic qualitative properties, has put in evidence the overall complexity of the bifurcation structure of the model, according also to recent works [23,49,42]. Local (stationary and Hopf) bifurcations have been determined analytically in this general framework; the next step consists in performing an analogous investigation for nonlocal and codimension-two bifurcations admitted by this general model; it will be a lot more challenging, and hopefully could give additional elements to try to explain phenomena still unclear in real ecosystems.

Acknowledgements

This work was performed in the frame of the activities sponsored by MIUR, by GNFM, by the University of Parma and Milano (Italy), and by CNR-IMATI. The authors are very grateful to the anonymous referees for their valuable comments and suggestions which helped them to considerably improve the paper.

Appendix A. List of main symbols

Symbol	Description
t	Time (d)
x	Ratio between prey biomass and maximum of prey population size
y	Ratio between predator biomass and maximum of prey population size
r_x	Maximum specific rate of prey growth (d^{-1})
b	Maximum specific rate of prey consumption (d^{-1})
m	Specific rate of predator mortality (d^{-1})
c	Conversion efficiency (from prey to predator biomass)
ϵ	Ratio between minimum and maximum of prey population size
$g(x)$	Adimensional function specifying the type of prey growth
$f\left(\frac{px}{1+hy}\right)$	Adimensional functional response of predator to prey abundance
p	Predation efficiency
h	Measure of the predator interference during the predation process
α	m/cb
β	$r_x c/m$
r_y	$cb - m$ (d^{-1})
p_0	$f^{-1}(\alpha)$
$\mu(s)$	$sf'(s)/f(s)$
μ_0	$\mu(p_0)$
γ	$c\mu_0/(1 - \mu_0)$
r_0	$m\mu_0/(1 - \mu_0)$ (d^{-1})
$\Lambda(h, p)$	$1 - \mu_0 - c\mu_0 hp_0/p$
$\phi(x, h)$	$1/x + h\beta g(x)$
$\psi(x)$	$\beta x^2 g'(x)$
ξ_0	Unique solution to $g'(x) = 0$
$\phi(\xi_0, h)$	$\beta h + 1/\xi_0$
η_0	Unique solution to $\psi'(x) = 0$

(continued on next page)

Symbol	Description
h_0	$1/\psi(\eta_0)$
h_1	$1/\psi(\epsilon)$
h_ϵ	Unique solution to $\phi_1(h) = 1/\epsilon$
η_1	Unique solution to $\psi(x) = 1/h_1$ in the range (η_0, ξ_0)
$\xi_1(h), \xi_2(h)$	Solutions to $\psi(x) = 1/h$, $\xi_1(h) \geq \xi_2(h)$
ϕ_0	$\phi(\eta_0, h_0)$
B_0	Cusp point $(h_0, p_0\phi_0)$
$\phi_j(h)$	$\phi(\xi_j(h), h)$, $j = 1, 2$
$p_1(h)$	Hopf bifurcation value for p
$p_2(h)$	Global bifurcation value for p
h_R	$1/(\xi_0(\gamma - \beta))$, unique solution to $\gamma h = \beta h + 1/\xi_0$
h_S	Unique solution to $\phi_1(h) = \gamma h$
h_U	Unique solution to $p_2(h) = p_0\phi_2(h)$
h_{BT}	Unique solution to $p_1(h) = p_0\phi_1(h)$

Appendix B. Details on some parameters

(i) Let

$$\mu(s) = \frac{sf'(s)}{f(s)}, \quad s > 0. \quad (\text{B.1})$$

From properties (5) and (9) it follows that

$$\mu(0) = 1, \quad 0 < \mu(s) < 1, \quad \lim_{s \rightarrow +\infty} \mu(s) = 0. \quad (\text{B.2})$$

The first two properties of $\mu(s)$ are easily verified. To prove the limit in (B.2), let us consider the identity

$$\int_{s_0}^s \frac{\mu(a)}{a} da = \int_{s_0}^s \frac{f'(a)}{f(a)} da, \quad (\text{B.3})$$

where $s_0 > 0$ is fixed, and $s > s_0$. From (B.3) we have that there exists $\hat{a}(s)$, $s_0 < \hat{a}(s) < s$, such that

$$\mu(\hat{a}(s)) = \frac{\log f(s)/f(s_0)}{\log s/s_0}. \quad (\text{B.4})$$

From (B.4), taking into account (5), it follows that

$$\lim_{s \rightarrow +\infty} \mu(\hat{a}(s)) = 0, \quad \lim_{s \rightarrow +\infty} \frac{\partial \mu(\hat{a}(s))}{\partial s} = \lim_{s \rightarrow +\infty} \frac{\mu(s) - \mu(\hat{a}(s))}{s \log s/s_0} = 0, \quad (\text{B.5})$$

which imply the limit in (B.2). However, from properties (5) we are not able to show the monotonicity condition $\mu'(s) < 0$, which holds for the functions $f(s)$ generally used in the applications.

- (ii) As a basic set of bioecological parameters to be used in numerical simulations, we have taken the values from Buffoni et al. [25], reported in the following table:

Parameter	r_x (d^{-1})	b (d^{-1}) (d^{-1})	m	c	ϵ
Value	0.11	0.88	0.19	0.39	0.2

These data have been estimated in [2]. They refer to an acarine system, surveyed in biological control field experiments: the phytophagous mite *Tetranychus urticae* and its biological control agent, the predator mite *Phytoseiulus persimilis* [2].

We wish to point out that, by using this choice of parameters, some relations, characterizing the ecological system, are satisfied. The inequality (15) $\alpha = m/(cb) = 0.55 < 1$ is fulfilled, and then non trivial dynamics can be found. The maximum growth rate r_x of the prey is less than the one of the predator:

$$r_x = 0.11 d^{-1} < r_y = cb - m = 0.15 d^{-1}.$$

With a Holling-type II trophic function we have that $r_0 = r_y$ (see Appendix C). It follows that in the (h, p) plane the two straight lines $p/p_0 = \gamma h$ and $p/p_0 = \beta h + 1/\xi_0$ intersect.

We have taken $r_x = 0.16 d^{-1}$ in some numerical experiments to simulate the case $r_x > r_y$.

Appendix C. Technical details of the stability analysis of the coexistence equilibrium state E_{*1}

We write here the expressions of the derivatives of $T(h, p, x_*)$ used in the following:

$$\frac{\partial T}{\partial h} = -r_x c \mu_0 \frac{p_0}{p} g(x_*) < 0, \quad \frac{\partial T}{\partial p} = r_x c \mu_0 \frac{p_0 h}{p^2} g(x_*) > 0, \quad (\text{C.1})$$

$$\frac{\partial T}{\partial x_*} = r_x \Lambda g'(x_*) + (x_* g'(x_*))'. \quad (\text{C.2})$$

We refer to Fig. 6 to illustrate the results of Theorem 2, relevant to the state $E_{*1}(h, p)$ when $r_x \geq r_0$, i.e. when $\beta \geq \gamma$ and the two lines $p/p_0 = \beta h + 1/\xi_0$ and $p/p_0 = \gamma h$ do not intersect.

Theorem 2. Assume (4)–(9) and $r_x \geq r_0$. Then, for any $h \geq 0$,

$$\exists p_1(h) : \quad p_0 \max\{1, \gamma h\} < p_1(h) < p_0 \left(\beta h + \frac{1}{\xi_0} \right),$$

such that

$$T(h, p_1(h), x_{*1}(p_1, h)) = 0, \quad T(h, p, x_{*1}(h, p)) < 0 \quad \text{for } p \in [p_0, p_1(h)),$$

and $T(h, p, x_{*1}(h, p)) > 0$ in the existence region of E_{*1} of the (h, p) plane where $p > p_1(h)$:

$$0 \leq h \leq h_0, \quad p_1(h) < p < \frac{p_0}{\epsilon} \quad \text{and} \quad h_0 < h, \quad p_1(h) < p < p_0 \phi_1(h).$$

Moreover,

$$\frac{dp_1}{dh} > 0.$$

Proof. From the implications (22) and (23) it follows that in the region $\boxed{1}$ of the (h, p) plane (Fig. 6)

$$h \geq \frac{1}{\gamma}, \quad 1 \leq \frac{p}{p_0} \leq \gamma h$$

we have

$$\Lambda \leq 0 \quad \text{and} \quad x_{*1} > \xi_0, \quad g'(x_{*1}) < 0,$$

which imply $T(h, p, x_{*1}) < 0$. Consider now the region $\square 2$ (Fig. 6)

$$\max\{1, \gamma h\} \leq \frac{p}{p_0} \leq \beta h + \frac{1}{\xi_0} < \phi_1(h).$$

On the boundaries we have that

$$T(h, p, x_{*1}) < 0 \quad \text{for} \quad \frac{p}{p_0} = \max\{1, \gamma h\},$$

where either $p = p_0$, $x_{*1}(h, p_0) = 1$ or $p = p_0 \gamma h$, $\xi_0 < x_{*1}(h, p_0 \gamma h) < 1$, and

$$T\left(h, p_0 \left(\beta h + \frac{1}{\xi_0}\right), \xi_0\right) > 0 \quad \text{for} \quad \frac{p}{p_0} = \beta h + \frac{1}{\xi_0}.$$

From the implications (22), (23) we have

$$\Lambda > 0 \quad \text{and} \quad x_{*1} > \xi_0, \quad g'(x_{*1}) < 0, \quad (x_{*1} g'(x_{*1}))' < 0.$$

Taking into account (C.1), (C.2), (22), (23) and the monotonicity property of x_{*1} ($\partial x_{*1} / \partial p < 0$), we have that

$$\frac{\partial T}{\partial x_{*1}} < 0, \quad \frac{dT}{dp} = \frac{\partial T}{\partial p} + \frac{\partial T}{\partial x_{*1}} \frac{\partial x_{*1}}{\partial p} > 0.$$

It follows that $T(h, p, x_{*1})$, considered as a function of p for fixed $h \geq 0$, is negative for $p/p_0 = \max\{1, \gamma h\}$, is increasing with p for $\max\{1, \gamma h\} < p/p_0 < \beta h + 1/\xi_0$ and positive for $p/p_0 = \beta h + 1/\xi_0$. Thus, there is just one zero of $T(h, p, x_{*1})$, denoted by $p_1(h)$, for $p_0 \max\{1, \gamma h\} < p < p_0(\beta h + 1/\xi_0)$.

Moreover, in the existence region $\square 3$ (Fig. 6) of E_{*1} of the (h, p) plane where $p > p_1(h)$ we have

$$\Lambda > 0 \quad \text{and} \quad x_{*1} < \xi_0, \quad g'(x_{*1}) > 0,$$

which imply $T(h, p, x_{*1}) > 0$.

Finally, the monotonicity property of $p_1(h)$ follows from $\partial T / \partial h < 0$. \square

When $r_x < r_0$, i.e. when $\beta < \gamma$ and the two lines $p/p_0 = \beta h + 1/\xi_0$ and $p/p_0 = \gamma h$ intersect at the point $h = h_R = 1/\xi_0(\gamma - \beta)$, Theorem 2 can be reformulated as follows. We refer to Fig. 7 to illustrate the results of Theorem 3.

Theorem 3. Assume (4)–(9) and $r_x < r_0$. Then,

(i) for $0 \leq h < h_R$, $\exists p_1(h) : p_0 \max\{1, \gamma h\} < p_1(h) < p_0 \left(\beta h + \frac{1}{\xi_0}\right)$, such that

$$T(h, p_1(h), x_{*1}(p_1, h)) = 0,$$

$$T(h, p, x_{*1}(h, p)) < 0 \quad \text{for} \quad p \in [p_0, p_1(h)), \quad h \geq 0$$

$$T(h, p, x_{*1}(h, p)) > 0 \quad \text{for} \quad 0 \leq h \leq h_0, \quad p_1(h) < p < \frac{p_0}{\epsilon} \quad \text{and}$$

$$h_0 < h < h_R, \quad p_1(h) < p < p_0 \phi_1(h).$$

Moreover,

$$\frac{dp_1}{dh} > 0.$$

(ii) A further region with positive trace is

$$h_R < h < h_S, \quad \gamma h < \frac{p}{p_0} < \phi_1(h),$$

where h_S is the unique solution to the equation $\gamma h = \phi_1(h)$.

The proof of [Theorem 3](#) is omitted because it follows the lines of the proof of the previous [Theorem 2](#).

The dynamical behaviours of predator–prey systems may be different depending on the sign of the difference $r_x - r_0$ and $r_x - r_y$, where r_0 is given in [\(25\)](#) and r_y in [\(14\)](#) [[47,48,50](#)]. With respect to this issue, we point out that with a Holling-type II trophic function the parameters p_0 and μ_0 are given by

$$p_0 = \frac{\alpha}{1 - \alpha}, \quad \mu_0 = 1 - \alpha,$$

so that

$$r_0 = \frac{m(1 - \alpha)}{\alpha} = r_y.$$

Otherwise, with an Ivlev trophic function we obtain

$$p_0 = -\ln(1 - \alpha), \quad \mu_0 = \frac{-(1 - \alpha) \ln(1 - \alpha)}{\alpha},$$

so that

$$r_0 = r_y \frac{-\alpha \ln(1 - \alpha)}{\alpha + (1 - \alpha) \ln(1 - \alpha)} > r_y.$$

References

- [1] J.A. Logan, Derivation and analysis of composite models for insect populations, in: *Estimation and Analysis of Insect Populations*, in: *Lecture Notes in Statistics*, vol. 55, Springer, 1989, pp. 278–288.
- [2] G. Buffoni, G. Gilioli, A lumped parameter model for acarine predator–prey population interactions, *Ecol. Modell.* 170 (2) (2003) 155–171.
- [3] P. Aguirre, E. González-Olivares, E. Sáez, Two limit cycles in a Leslie–Gower predator–prey model with additive Allee effect, *Nonlinear Anal. RWA* 10 (3) (2009) 1401–1416.
- [4] D.S. Boukal, L. Berec, Modelling mate-finding Allee effects and populations dynamics, with applications in pest control, *Popul. Ecol.* 51 (3) (2009) 445–458.
- [5] M.E. Gilpin, A model of the predator–prey relationship, *Theor. Popul. Biol.* 5 (3) (1974) 333–344.
- [6] E. Kuno, Principles of predator–prey interaction in theoretical, experimental and natural population system, *Adv. Ecol. Res.* 16 (1987) 249–337.
- [7] P.A. Stephens, W.J. Sutherland, R.P. Freckleton, What is the Allee effect? *Oikos* 87 (1999) 185–190.
- [8] C.M. Taylor, A. Hastings, Allee effects in biological invasions, *Ecol. Lett.* 8 (8) (2005) 895–908.
- [9] M.E. Gilpin, M.E. Soulé, Minimum viable populations: processes of species extinction, in: M. Soulé (Ed.), *Conservation Biology: The Science of Scarcity and Diversity*, Sinauer Associates, Sunderland, Massachusetts, 1986, pp. 13–34.
- [10] A. Yablokov, *Population Biology: Progress and Problems of Studies on Natural Populations*, MIR Publishers, Moscow, 1986.
- [11] Y. Svirezhev, D. Logofet, *Stability of Biological Communities*, Vol. 112, MIR Publishers, Moscow, 1983.
- [12] G. Buffoni, M. Groppi, C. Soresina, Effects of prey over-crowding in predator–prey systems with prey-dependent trophic functions, *Nonlinear Anal. RWA* 12 (5) (2011) 2871–2887.
- [13] A.D. Bazykin, *Nonlinear Dynamics of Interacting Populations*, Vol. 11, World Scientific, Singapore, 1998.
- [14] C.S. Holling, The functional response of invertebrate predators to prey density, *Mem. Entomol. Soc. Can.* 98 (1966) 5–86.
- [15] V. Ivlev, *Experimental Ecology of the Feeding of Fishes*, Vol. 42, Yale University Press, New Haven, CT, 1961.
- [16] T. Royama, A comparative study of models for predation and parasitism, *Res. Popul. Ecol.* S1 (1971) 1–91.
- [17] R. Arditi, L.R. Ginzburg, Coupling in predator–prey dynamics: ratio-dependence, *J. Theoret. Biol.* 139 (3) (1989) 311–326.
- [18] A.A. Berryman, The origins and evolution of predator–prey theory, *Ecology* 73 (5) (1992) 1530–1535.
- [19] L.R. Ginzburg, H.R. Akçakaya, Consequences of ratio-dependent predation for steady-state properties of ecosystems, *Ecology* 73 (5) (1992) 1536–1543.
- [20] D.S. Boukal, M.W. Sabelis, L. Berec, How predator functional responses and Allee effects in prey affect the paradox of enrichment and population collapses, *Theor. Popul. Biol.* 72 (1) (2007) 136–147.

- [21] A. Gutierrez, Physiological basis of ratio-dependent predator–prey theory: the metabolic pool model as a paradigm, *Ecology* 73 (5) (1992) 1552–1563.
- [22] F. Berezovskaya, G. Karev, R. Arditi, Parametric analysis of the ratio-dependent predator–prey model, *J. Math. Biol.* 43 (3) (2001) 221–246.
- [23] P. Aguirre, A general class of predation models with multiplicative Allee effect, *Nonlinear Dynam.* 78 (1) (2014) 629–648.
- [24] L. Van Coller, Automated techniques for the qualitative analysis of ecological models: continuous models, *Conserv. Ecol.* 1 (1) (1997) 5. Available from <http://www.ecologyandsociety.org/vol1/iss1/art5/>.
- [25] G. Buffoni, M.P. Cassinari, M. Groppi, M. Serluca, Modelling of predator–prey trophic interactions. Part I: two trophic levels, *J. Math. Biol.* 50 (6) (2005) 713–732.
- [26] P.A. Abrams, L.R. Ginzburg, The nature of predation: prey dependent, ratio dependent or neither? *Trends Ecol. Evol.* 15 (8) (2000) 337–341.
- [27] J. Beddington, Mutual interference between parasites or predators and its effect on searching efficiency, *J. Anim. Ecol.* 44 (1975) 331–340.
- [28] D.L. DeAngelis, R. Goldstein, R. O’Neill, A model for trophic interaction, *Ecology* 56 (1975) 881–892.
- [29] A. Gutierrez, J. Baumgärtner, Multitrophic level models of predator–prey energetics: II. A realistic model of plant–herbivore–parasitoid–predator interactions, *Can. Entomol.* 116 (7) (1984) 933–949.
- [30] G. Seo, D.L. DeAngelis, A predator–prey model with a Holling type I functional response including a predator mutual interference, *J. Nonlinear Sci.* 21 (6) (2011) 811–833.
- [31] H. Freedman, J.-H. So, Global stability and persistence of simple food chains, *Math. Biosci.* 76 (1) (1985) 69–86.
- [32] L. Perko, *Differential Equations and Dynamical Systems*, Springer-Verlag, New York, 1991.
- [33] V.I. Arnol’d, *Catastrophe Theory*, Springer-Verlag, Berlin, 1992.
- [34] J. Guckenheimer, P. Holmes, *Nonlinear Oscillations, Dynamical Systems, and Bifurcations of Vector Fields*, Vol. 42, Springer Verlag, New York, 1983.
- [35] Y.A. Kuznetsov, *Elements of Applied Bifurcation Theory*, Vol. 112, Springer Verlag, New York, 1998.
- [36] A. Dhooge, W. Govaerts, Y.A. Kuznetsov, Matcont: A MATLAB package for numerical bifurcation analysis of ODEs, *ACM Trans. Math. Software* 29 (2) (2003) 141–164. Software available from <http://www.matcont.ugent.be/>.
- [37] P. Aguirre, E. González-Olivares, E. Sáez, Three limit cycles in a Leslie–Gower predator–prey model with additive Allee effect, *SIAM J. Appl. Math.* 69 (5) (2009) 1244–1262.
- [38] P. Aguirre, J.D. Flores, E. González-Olivares, Bifurcations and global dynamics in a predator–prey model with a strong Allee effect on the prey, and a ratio-dependent functional response, *Nonlinear Anal. RWA* 16 (2014) 235–249.
- [39] M. Sen, M. Banerjee, A. Morozov, Bifurcation analysis of a ratio-dependent prey–predator model with the Allee effect, *Ecol. Complex.* 11 (2012) 12–27.
- [40] J.D. Flores, E. González-Olivares, Dynamics of a predator–prey model with Allee effect on prey and ratio-dependent functional response, *Ecol. Complex.* 18 (2014) 59–66.
- [41] Y. Gao, B. Li, Dynamics of a ratio-dependent predator–prey system with a strong Allee effect, *Discrete Contin. Dyn. Syst. Ser. B* 18 (9) (2013) 2283–2313.
- [42] M. Adamson, A.Y. Morozov, Bifurcation analysis of models with uncertain function specification: How should we proceed? *Bull. Math. Biol.* 76 (5) (2014) 1218–1240.
- [43] G.A. Van Voorn, L. Hemerik, M.P. Boer, B.W. Kooi, Heteroclinic orbits indicate overexploitation in predator–prey systems with a strong Allee effect, *Math. Biosci.* 209 (2) (2007) 451–469.
- [44] J. Zu, Global qualitative analysis of a predator–prey system with Allee effect on the prey species, *Math. Comput. Simul.* 94 (2013) 33–54.
- [45] S. Nundloll, L. Mailleret, F. Grogard, Influence of intrapredatory interferences on impulsive biological control efficiency, *Bull. Math. Biol.* 72 (8) (2010) 2113–2138.
- [46] J. Zu, M. Mimura, The impact of Allee effect on a predator–prey system with Holling type II functional response, *Appl. Math. Comput.* 217 (7) (2010) 3542–3556.
- [47] G. Buffoni, M.P. Cassinari, M. Groppi, Modelling of predator–prey trophic interactions. Part II: three trophic levels, *J. Math. Biol.* 54 (5) (2007) 623–644.
- [48] Y.A. Kuznetsov, S. Rinaldi, Remarks on food chain dynamics, *Math. Biosci.* 134 (1) (1996) 1–33.
- [49] M. Adamson, A.Y. Morozov, When can we trust our model predictions? Unearthing structural sensitivity in biological systems, *Proc. R. Soc. Lond. Ser. A Math. Phys. Eng. Sci.* 469 (2012) 20120500.
- [50] K. McCann, P. Yodzis, Biological conditions for chaos in a three-species food chain, *Ecology* 75 (1994) 561–564.